

# Core–Periphery Structure in Directed Networks

Andrew Elliott<sup>1,2</sup>, Angus Chiu<sup>2</sup>, Marya Bazzi<sup>1,3,4</sup>,  
Gesine Reinert<sup>1,2</sup> and Mihai Cucuringu<sup>1,2,4</sup>

<sup>1</sup> The Alan Turing Institute, London, UK <sup>2</sup> Department of Statistics, University of Oxford, UK

<sup>3</sup> Mathematical Institute, University of Warwick, UK <sup>4</sup> Mathematical Institute, University of Oxford, UK

## Abstract

While studies of meso-scale structures in networks often focus on community structure, core–periphery structures can reveal new insights. This structure typically consists of a well-connected core and a periphery that is well connected to the core but sparsely connected internally. Most studies of core–periphery structure focus on undirected networks.

We propose a generalisation of core–periphery structure to directed networks. Our approach yields a family of core–periphery block model formulations in which core and periphery sets are edge-direction dependent. We mainly focus on a particular core–periphery structure consisting of two core sets and two periphery sets which we motivate empirically.

To detect this directed core–periphery structure we propose four different methods, with different trade-offs between computational complexity and accuracy. We assess these methods on three benchmarks and compare to four standard methods. On simulated data, the proposed methods match or outperform the standard methods. Applying our methods to three empirical networks – a political blogs networks, a faculty hiring network, and a trade network – illustrates that this directed core–periphery structure can offer novel insights about the underlying dataset.

## 1 Introduction

Networks provide useful representations of complex systems across many applications [36], such as physical, technological, information, biological, financial, and social systems. A network in its simplest form is a graph in which vertices represent entities of interest and edges represent pairwise interactions of interest. In weighted graphs, each edge has an associated edge weight; in an unweighted graph, the edge weights are 0 (absent) or 1 (present). Edges can also incorporate directions to represent asymmetric interactions; here, we consider directed unweighted networks (with some methods adaptable to weighted networks).

Given a network representation of a system, it can be useful to apply coarse-graining techniques to investigate so-called meso-scale features that lie between the micro-scale (local vertex properties e.g. subgraph counts) and the macro-scale (global network properties e.g., total edge weight, degree distribution, average local clustering coefficient). Typical meso-scale structures are community structure, core–periphery structure, role structure, and hierarchical structure [36, 43, 40, 5]; often, more than one of these is present in a network, see for example [40]. Communities are the most commonly studied type of meso-scale structure. A community is loosely defined as a set of vertices that are more densely connected to each other than they are to vertices in the rest of the network. Many algorithms have been developed to detect communities, which have led to insights in a wide variety of applications, see for example [41, 18, 36].

In the present paper, we focus on core–periphery structure. The concept of core–periphery stems from studies of economic and social networks [43], and was first formalised by Borgatti and Everett [7]. Typically, core–periphery structure is a partition of an undirected network into two sets, a core and a periphery, such that there are dense connections within the core and sparse connections within the periphery [7]. Furthermore, core vertices are reasonably well-connected to the periphery vertices. Extensions allow for multiple core–periphery pairs and nested core–periphery structures [16, 26, 40]. Many algorithms have been developed for detecting (different variants) of core–periphery structure. These include approaches based on the optimisation of a quality function [7, 43, 20, 50, 52, 40], spectral methods [15, 47, 35], and notions of core–periphery based on transport (e.g., core vertices are likely to be on many shortest paths between other vertices in the network) rather than edge densities and weights [15, 29]. Core–periphery detection has been applied to various fields such as economics, sociology, international relations, journal-to-journal networks, and networks of interactions between scientists; see [46] for a recent survey.

Many methods for detecting core–periphery were developed for undirected networks, and although they can be (and some have been) generalised to directed graphs, they do not also generalise the definition of a discrete core and periphery to be edge-direction dependent, but rather, either disregard the edge-direction or consider the edge in each direction as an independent observation [40, 3, 48, 7] or use a continuous structure [9].

To the best of our knowledge, the only structure that can be interpreted as a form of generalisation of core–periphery structure to directed networks where the definition of core and periphery is edge-direction dependent, is the bow-tie structure [13, 10]. Bow-tie structure consists of a core (defined as the largest connected component), an in-periphery (all vertices with a directed path to a vertex in the core), an out-periphery (all vertices with a directed path from a vertex in the core), and other sets containing any remaining vertices [10, 30, 51].

In this paper, we introduce a generalisation of the block-model core–periphery structure introduced in [7] to directed networks, in which the definition of both core and periphery are edge-direction dependent. We propose four methods to detect the proposed directed core–periphery structure, and illustrate their performance on synthetic and empirical networks. We include comparisons to bow-tie structure in our synthetic experiments and illustrate that the structure we propose yields additional insights about empirical networks. Moreover, we suggest a framework for defining cores and peripheries in way that accounts for edge direction, which yields as special cases a bow-tie-like structure and the structure we focus on in the present paper.

This paper is organised as follows. In Section 2 we introduce a novel block-model for directed core–periphery structure that consists of four sets (two periphery sets and two core sets) and a two-parameter synthetic model that can generate the proposed structure. In Section 3 we introduce four methods for detecting the proposed directed core–periphery structure. The first one is a generalisation of the low-rank approximation approach introduced in [15] (see Section 3.1), the second and third are adaptations and extensions of the HITS algorithm [23] (see Section 3.2), and the fourth is a likelihood-maximisation approach (see Section 3.3). Section 4 illustrates the performance of our methods on synthetic benchmark networks. In Section 5, we apply the methods to three real-world data sets. Section 6 summarises our main results and offers directions for future work.

The code for our proposed methods and the implementation for bow-tie structure is available at <https://github.com/alan-turing-institute/directedCorePeripheryPaper>.

## 2 Core–periphery structure

**Core–periphery structure in undirected networks** The most well-known quantitative formulation of core–periphery structure was introduced by Borgatti and Everett [7]. They propose both a discrete and a continuous model for detecting core–periphery structure in undirected networks. We describe below the (discrete) block model formulation introduced in [7], which we generalise to directed networks later in this section.

In the discrete notion of core–periphery structure, [7] suggests that a core–periphery model should consist of two sets: a densely connected core and a loosely connected periphery, with dense connections between the core and the periphery. Formally, let  $n_c$  denote the number of vertices in the core and  $n_p$  the number of vertices in the periphery, with  $n_c + n_p = n$  (i.e., the core and the periphery form a partition of the vertices in the graph). The idealised probability matrix and network representation that match the undirected core–periphery structure is given by

$$\mathbf{M}_0 = \begin{array}{c|cc} & \text{Core} & \text{Periphery} \\ \hline \text{Core} & 1 & 1 \\ \text{Periphery} & 1 & 0 \end{array} \quad \begin{array}{c} \circ \\ \text{Core} \text{---} \text{Per.} \end{array} \quad (1)$$

with corresponding adjacency matrix

$$\mathbf{A}_0 = \begin{array}{|cc|} \hline \mathbf{1}_{n_c \times n_c} & \mathbf{1}_{n_c \times n_p} \\ \hline \mathbf{1}_{n_p \times n_c} & \mathbf{0}_{n_p \times n_p} \\ \hline \end{array}, \quad (2)$$

where  $\mathbf{1}_{n_1 \times n_2}$  (respectively,  $\mathbf{0}_{n_1 \times n_2}$ ) denotes an  $n_1 \times n_2$  matrix in which every entry takes the value 1 (respectively, 0). In adjacency matrices of real-world data sets, any structure of the form Eq. (2), if present, is likely observed with random noise. With  $\text{sgn}$  denoting the signum function that maps a real number to 1 if the number is positive, to  $-1$  if the number is negative, and to 0 if the number is zero, the block matrix  $\mathbf{A}_0$  is equivalent (up to row and column permutations) to the matrix with  $(i, j)^{\text{th}}$  entry  $\text{sgn}(x_i + x_j)$ , with  $x_i = 1$  if  $i$  is in the core and 0 otherwise [47]. To detect core–periphery structure in a graph with adjacency matrix  $\mathbf{A} \in \{0, 1\}^{n \times n}$ , one approach introduced in [7], see also [47], is to optimise the quality function

$$\sum_{i,j=1}^n A_{ij} \text{sgn}(x_i + x_j), \quad (3)$$

over  $\mathbf{x} = (x_1, \dots, x_n) \in \Omega = \{\mathbf{x} \in \{0, 1\}^n \mid \sum_{i=1}^n x_i = n_c\}$  for a fixed  $n_c \in \mathbb{N}$ . The intuition is that the larger the double summation in Eq. (3), the greater the extent to which the adjacency matrix matches the idealised block matrix in Eq. (2). One can use (3) to detect core–periphery structure in weighted and directed networks [7], and different detection methods for undirected networks build on this formulation by changing the signum function in Eq. (3) [7, 47, 43].

**Core–periphery structure in directed networks** Now we introduce a block model for directed core–periphery in which the definitions of the core and periphery sets are edge-direction-dependent. To incorporate information about edge direction in the formulation of the block model itself, we split each of the sets in Eq. (2) into one that has incoming edges and another one that has outgoing edges. This yields four sets in total, which we denote  $\mathcal{C}_{in}$  (*core-in*),  $\mathcal{C}_{out}$  (*core-out*),  $\mathcal{P}_{in}$

(*periphery-in*) and  $\mathcal{P}_{out}$  (*periphery-out*). Within each of the two core sets ( $\mathcal{C}_{in}$  and  $\mathcal{C}_{out}$ ) and periphery sets ( $\mathcal{P}_{in}$  and  $\mathcal{P}_{out}$ ), we adopt the same convention as in Eq. (2): the two core sets are fully internally connected and the two periphery sets have no internal edges. In line with the intuition behind core–periphery structure, we also assume that edges do not exist between the periphery sets. There are no multiple edges, but there are self-loops. Specifically, we assume the following block probability matrix and corresponding network representation

$$\mathbf{M} = \begin{array}{c|cccc} & \mathcal{P}_{out} & \mathcal{C}_{in} & \mathcal{C}_{out} & \mathcal{P}_{in} \\ \hline \mathcal{P}_{out} & 0 & \mathbf{1} & 0 & 0 \\ \mathcal{C}_{in} & 0 & \mathbf{1} & 0 & 0 \\ \mathcal{C}_{out} & 0 & \mathbf{1} & \mathbf{1} & \mathbf{1} \\ \mathcal{P}_{in} & 0 & 0 & 0 & 0 \end{array} \quad \begin{array}{c} \boxed{\mathcal{P}_{out}} \\ \downarrow \\ \boxed{\mathcal{C}_{in}} \\ \uparrow \\ \boxed{\mathcal{C}_{out}} \\ \downarrow \\ \boxed{\mathcal{P}_{in}} \end{array} \quad (4)$$

To gain some empirical intuition for the structure in Eq. (4), we motivate it with a few real-world examples. Consider networks that represent a type of information flow, with two sets that receive information ( $\mathcal{C}_{in}$  and  $\mathcal{P}_{in}$ ) and two sets that transmit/send information ( $\mathcal{C}_{out}$  and  $\mathcal{P}_{out}$ ). Furthermore, within each of these categories, there is one set with core-like properties and another one with periphery-like properties. Inspired by [5], in a Twitter network for example,  $\mathcal{C}_{in}$  and  $\mathcal{P}_{in}$  could correspond to consumers of information, with  $\mathcal{C}_{in}$  having the added property of being a closely-knit community that has internal discussions (e.g., interest groups) rather than individuals collecting information independently (e.g., an average user). On the other hand,  $\mathcal{C}_{out}$  and  $\mathcal{P}_{out}$  could correspond to transmitters of information, with  $\mathcal{C}_{out}$  having the added property of being a well-known closely-knit community (e.g., broadcasters) rather than individuals spreading information independently (e.g., celebrities). Another class of examples is networks that represent a type of social flux, when there are two sets that entities move out of, and two sets that entities move towards. Furthermore, within each of these categories, there is one with core-like properties and one with periphery-like properties. In a faculty hiring network of institutions for example,  $\mathcal{C}_{out}$  may correspond to highly-ranked institutions with sought-after alumni, while  $\mathcal{C}_{in}$  may correspond to good institutions which take in more faculty than they let go. For the periphery sets,  $\mathcal{P}_{out}$  may correspond to lower-ranked institutions which do not attract faculty from higher-ranked institutions, and  $\mathcal{P}_{in}$  may correspond to a set of institutions which attract many alumni from highly-ranked ones. These ideas will be illustrated on real-world data in Section 5.

While the extension of Eq. (1) in Eq. (4) can be regarded as a natural one to consider in that the edge-direction dependence is defined in the same way for both core and periphery sets, there are other choices that one can pursue. In Supplementary Information (SI) A, a framework is provided from which one can derive a set of directed core–periphery structures of which Eq. (4) is one example; they also include a block model formulation of bow-tie structure.

**Synthetic model for directed core–periphery structure** Here we describe a stochastic block model that we will use as a synthetic graph model to benchmark our methods. Consider a partition with four sets, namely  $\mathcal{P}_{out}$ ,  $\mathcal{C}_{in}$ ,  $\mathcal{C}_{out}$  and  $\mathcal{P}_{in}$  with respective sizes  $n_{\mathcal{P}_{out}}$ ,  $n_{\mathcal{C}_{in}}$ ,  $n_{\mathcal{C}_{out}}$  and  $n_{\mathcal{P}_{in}}$ . For any two vertices  $u, v$  let  $X(u, v)$  be the random variable which equals 1 if there is an edge from  $u$  to  $v$ , and 0 otherwise. We refer to  $X(u, v)$  as an *edge indicator*. For an edge indicator which should equal 1 according to the perfect structure (Eq. (4)) let  $p_1$  be the probability that an edge is observed. Similarly for an edge indicator which should be 0 according to the perfect structure (Eq. (4)) let  $p_2$  be the probability that an edge is observed. Thinking of  $p_2$  as noise and of  $p_1$  as

signal, we assume that  $p_1 > p_2$  so that the noise does not overwhelm the structure Eq. (4). We represent this model as a stochastic block model with probability matrix

$$p_1 \mathbf{M} + p_2 (\mathbf{1} - \mathbf{M}) = \begin{pmatrix} p_2 & p_1 & p_2 & p_2 \\ p_2 & p_1 & p_2 & p_2 \\ p_2 & p_1 & p_1 & p_1 \\ p_2 & p_2 & p_2 & p_2 \end{pmatrix}, \quad (5)$$

where  $\mathbf{1} = \mathbf{1}_{4 \times 4}$ . Setting  $p_1 = 1$  and  $p_2 = 0$  recovers the idealised block structure in Eq. (4). This two-parameter model allows to increase the difficulty of the detection by reducing the difference between  $p_1$  and  $p_2$ , and to independently modify the expected density of edges matching (respectively, not matching) the planted structure by varying  $p_1$  (respectively,  $p_2$ ).

A special case of Eq. (5) with  $p_1 = 0.5 + p$  and  $p_2 = 0.5 - p$ ,  $p \in [0, 0.5]$ , yields the stochastic block model with probability matrix

$$(0.5 + p) \mathbf{M} + (0.5 - p) (\mathbf{1} - \mathbf{M}). \quad (6)$$

This model yields the idealised block structure in Eq. (4) when  $p = 0.5$  and an Erdős-Rényi random graph when  $p = 0$ . By varying  $p$  between these bounds, one simultaneously varies the expected density of edges that match the planted structure.

Examples of both model instances are shown in the first row of Fig. 1. The first three panels of the first row of Fig. 1 show example adjacency matrices obtained with Eq. (5),  $n = 400$ , and equally-sized  $n_{\mathcal{P}_{out}} = n_{\mathcal{C}_{in}} = n_{\mathcal{C}_{out}} = n_{\mathcal{P}_{in}} = 100$ . We fix  $p_2 = 0.1$  and vary  $p_1$ . As  $p_1$  decreases with fixed  $p_2$ , the ‘L’-shaped pattern starts to fade away and the sparseness of the network increases. The last three panels show realisations of adjacency matrices obtained with Eq. (6) for  $p \in \{0.1, 0.3, 0.45\}$ ,  $n = 400$ , and four equally-sized blocks. As anticipated, the ‘L’-shaped pattern is less clear for larger values of  $p$ . We shall return to Fig. 1 in the next section.

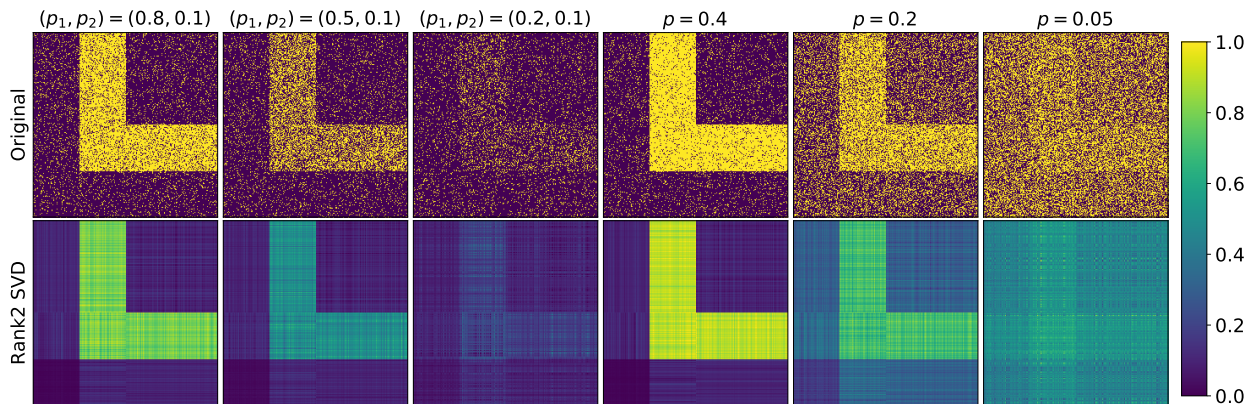


Figure 1: Heatmaps illustrating our model and the rank-2 SVD approximation. Top row: heatmaps of the original adjacency matrix, with  $n = 400$  vertices. We generate the first three examples with (5) and the second three examples with (6), for which  $p_1 = 0.5 + p$  and  $p_2 = 0.5 - p$ . Blocks are equally-sized in both cases. Bottom row: heatmaps of the low-rank SVD reconstruction for the adjacency matrix above it.

### 3 Core–periphery detection in directed networks

The directed core–periphery block structure in Eq. (4) differs from the original undirected core–periphery structure in Eq. (1) in two important ways: the structure in Eq. (4) is asymmetric, and it consists of two core sets and two periphery sets, each with their own distinct characteristics. In this section, we describe three method classes for detecting this novel structure, ordered by run time, from fast to slow. From these three method classes we shall select four methods for directed core–periphery detection. The first is based on a generalisation of the low-rank approximation approach in [15], the second and third are based on an adaptation of the popular HITS algorithm [23], and the fourth is based on likelihood-maximisation.

#### 3.1 Method class 1: Low-rank approximation

Our first approach generalises the low-rank approximation method which was developed for undirected networks in [15]. For a low-rank approximation of an asymmetric matrix, the singular value decomposition (SVD) of the  $n \times n$  adjacency matrix  $\mathbf{A}$  is given by  $\mathbf{A} = \mathbf{U}\mathbf{\Sigma}\mathbf{V}^T$ , where  $\mathbf{U}$  (left-singular vectors) and  $\mathbf{V}$  (right singular vectors) are orthogonal  $n \times n$  matrices and  $\mathbf{\Sigma}$  is a  $n \times n$  diagonal matrix with the so-called singular values on the diagonal. Singular values are real and non-negative, and by convention, sorted in descending order. For a rank- $r$  approximation, we keep the top  $r$  singular vectors of  $\mathbf{U}$  and  $\mathbf{V}$ . Formally, let  $\mathbf{U}_r$  (respectively,  $\mathbf{V}_r$ ) be a  $n \times r$  (respectively,  $r \times n$ ) matrix storing the first  $r$  columns of  $\mathbf{U}$  (respectively,  $\mathbf{V}$ ), and let  $\mathbf{\Sigma}_r$  be a  $r \times r$  matrix constructed from the first  $r$  rows and columns of  $\mathbf{\Sigma}$ . A rank- $r$  approximation of  $\mathbf{A}$  is

$$\hat{\mathbf{A}} = \mathbf{U}_r \mathbf{\Sigma}_r \mathbf{V}_r^T, \quad (7)$$

the matrix of rank  $r$  with the lowest possible Frobenius error, by the Eckart-Young theorem.

Similarly to the undirected case in [15], one can interpret a low-rank approximation as a ‘denoising’ of the original adjacency matrix. The appropriate rank of approximation for detecting a given structure is dictated by the rank of the idealised block model. The rank-2 block matrix in Eq. (4) would suggest a rank-2 approximation. The second row of Fig. 1 shows the rank-2 approximations for the synthetic adjacency matrices in the first row of Fig. 1. In all of these cases, a rank-2 approximation of the adjacency matrix is able to highlight the planted ‘L’ structure.

To partition the network vertex set into  $\mathcal{P}_{out}$ ,  $\mathcal{C}_{in}$ ,  $\mathcal{C}_{out}$  and  $\mathcal{P}_{in}$  based on the low-rank approximation in Eq. (7) with  $r = 2$ , we use a score which is analogous to the degree-based score of [15] for the undirected case. Let the in- or out-degree of a set be the sum of the in- or out-degrees of its vertices. In a network which perfectly matches the directed core-periphery structure (4), the in-degree of  $\mathcal{P}_{out}$  would be 0, the out-degree of  $\mathcal{P}_{in}$  would be 0, the in-degree of  $\mathcal{C}_{in}$  would equal  $(n_{\mathcal{P}_{out}} + n_{\mathcal{C}_{out}} + n_{\mathcal{C}_{in}}) n_{\mathcal{C}_{in}}$ , and also the out-degree of  $\mathcal{C}_{out}$  would equal  $(n_{\mathcal{P}_{in}} + n_{\mathcal{C}_{out}} + n_{\mathcal{C}_{in}}) n_{\mathcal{C}_{out}}$ . We denote by  $C_{in}^{LR}(i)$  the  $\mathcal{C}_{in}$  score of vertex  $i$  with respect to our low rank method, with equivalent formulations for the remaining sets. Based on the idealised block structure in Eq. (4),  $\mathcal{C}_{in}$  should have the highest number of incoming edges and  $\mathcal{C}_{out}$  the highest number of out-going edges. Accordingly, one would expect a vertex  $i$  to contribute more to the  $C_{in}^{LR}$  score if it has high in-degree, and to contribute more to the  $C_{out}^{LR}$  score if it has high out-degree. We thus set

$$C_{in}^{LR}(i) = \sum_{j=1}^n \hat{A}_{ji}, \quad C_{out}^{LR}(i) = \sum_{j=1}^n \hat{A}_{ij}, \quad (8)$$

which yield the in-degree and out-degree, respectively, of vertex  $i$  in the network with adjacency matrix  $\hat{\mathbf{A}}$  from Eq. (7). Similarly, based on the idealised structure in Eq. (4), a vertex should have a high  $\mathbf{P}_{in}^{LR}$  score if it has low out-degree compared to the maximal out-degree, and a vertex should have a high  $\mathbf{P}_{out}^{LR}$  score if it has low in-degree compared to the maximal in-degree. We set

$$P_{in}^{LR}(i) = \max_j \left( \sum_{a=1}^n \hat{A}_{ja} \right) - \sum_{a=1}^n \hat{A}_{ia} = \max_j (C_{out}^{LR}(j)) - C_{out}^{LR}(i), \quad (9)$$

$$P_{out}^{LR}(i) = \max_j \left( \sum_{a=1}^n \hat{A}_{aj} \right) - \sum_{a=1}^n \hat{A}_{ai} = \max_j (C_{in}^{LR}(j)) - C_{in}^{LR}(i). \quad (10)$$

In SI C we consider alternative variants of these scores and note that the above scores achieve the best performance on the synthetic benchmarks.

To convert the scores into a partition of a network, we consider the  $n \times 4$  score matrix  $\mathbf{S}^{LR} = [\mathbf{P}_{out}^{LR}, \mathbf{C}_{in}^{LR}, \mathbf{C}_{out}^{LR}, \mathbf{P}_{in}^{LR}]$ . We normalise each row of  $\mathbf{S}^{LR}$  such that it has an  $L_2$ -norm of 1. Heuristically the normalisation allows the rows of  $\mathbf{S}^{LR}$  (vectors in 4-dimensional space) not only to concentrate in four different directions, but to do so while also having a small within-set Euclidean distance [14, 28]. We then partition the vertices by clustering  $\mathbf{S}^{LR}$  using k-means++ [2], a variant of the popular k-means clustering algorithm that alleviates the issues of unstable clusterings retrieved by k-means [32]. We refer to this method as LOWRANK.

### 3.2 Method class 2: The Hyperlink-Induced Topic Search (HITS) algorithm

Our second method builds on a well-known algorithm in link analysis known as Hyperlink-Induced Topic Search (HITS) [23]. Similarly to PageRank, the HITS algorithm was originally designed to measure the importance of webpages or other documents using the structure of the directed links between the webpages [8]. The underlying intuition is that authoritative webpages on a topic should not only have large in-degrees (i.e., they constitute hyperlinks on many webpages) but should also considerably overlap in the sets of pages that point to them. There exists a mutually reinforcing relationship between authoritative webpages for a topic, referred to as “authorities”, and pages that link to many related authorities, referred to as “hubs”. A good hub is a page that points to many good authorities, and a good authority is a page that is pointed to by many good hubs. Consequently, the HITS algorithm assigns to each webpage two vertex-based scores the “authority scores”  $\mathbf{a}$  and the “hub scores”  $\mathbf{h}$ , with the following recursive relationship  $\mathbf{a} = \mathbf{A}^T \mathbf{h}$  and  $\mathbf{h} = \mathbf{A} \mathbf{a}$ . The HITS algorithm determines the scores iteratively. Initially, all authority and hub scores are set to  $\mathbf{1}_n$ . At each iteration of the HITS algorithm, one sequentially updates the authority and hub scores. A normalisation step is then applied, so that the vectors  $\mathbf{a}$  and  $\mathbf{h}$  become unit vectors in some norm [8]. Kleinberg [23] proves that the algorithm converges to the principal left and right singular vectors of the adjacency matrix  $\mathbf{A}$ , provided that the initial authority and hub vectors are not orthogonal to the principal eigenvectors of  $\mathbf{A}^T \mathbf{A}$  and  $\mathbf{A} \mathbf{A}^T$ .

We use this method in two ways: (i) we construct a score based directly on the hub and authority scores, (ii) we generalise this method from the case of two scores (hub and authority) to the case of four scores, motivated by the four sets in our directed core-periphery structure.

**Direct use of HITS scores.** To construct the  $\mathbf{C}_{in}^{HITS}$ ,  $\mathbf{C}_{out}^{HITS}$ ,  $\mathbf{P}_{in}^{HITS}$ ,  $\mathbf{P}_{out}^{HITS}$  scores, we begin by noting that a vertex would have a high authority score if it has many incoming edges, whereas it

would have a high hub score if it has many outgoing edges. Based on the idealised block structure in Eq. (4), vertices with the highest authority scores should also have a high  $\mathbf{C}_{in}^{HITS}$  score, and vertices with the highest hub scores should also have a high  $\mathbf{C}_{out}^{HITS}$  score. We let

$$C_{in}^{HITS}(i) = h(i) \quad \text{and} \quad C_{out}^{HITS}(i) = a(i).$$

To set the remaining scores we use the same intuition as for the low-rank setting, and let

$$P_{in}^{HITS}(i) = \max_j(C_{out}^{HITS}(j)) - C_{out}^{HITS}(i), \quad (11)$$

$$P_{out}^{HITS}(i) = \max_j(C_{in}^{HITS}(j)) - C_{in}^{HITS}(i). \quad (12)$$

We then cluster the resulting scores using the same procedure used for LOWRANK (see Section 33.1), and following LOWRANK we refer to this method as HITS. Recalling the relation between the HITS algorithm and SVD from Kleinberg [24], our score based on the HITS algorithm can be construed as a variant of LOWRANK, in which we only consider a rank-1 approximation and use the SVD components directly.

**An alternative 4 score scheme ADVHITS (Advanced Hits).** Instead of using hub and authority scores, in each set, edge indicators are rewarded when they match the structure in Eq. (4) and penalised otherwise, through the reward-penalty matrix associated to  $\mathbf{M}$  given by

$$\mathbf{D} = 2\mathbf{M} - \mathbf{1} = \begin{vmatrix} -1 & \mathbf{1} & -1 & -1 \\ -1 & \mathbf{1} & -1 & -1 \\ -1 & \mathbf{1} & \mathbf{1} & \mathbf{1} \\ -1 & -1 & -1 & -1 \end{vmatrix} = \begin{vmatrix} \mathbf{d}_1 & \mathbf{d}_2 & \mathbf{d}_3 & \mathbf{d}_4 \end{vmatrix} = \begin{vmatrix} \mathbf{e}_1 \\ \mathbf{e}_2 \\ \mathbf{e}_3 \\ \mathbf{e}_4 \end{vmatrix},$$

where  $\mathbf{d}_i$  is the  $i^{\text{th}}$  column vector of  $\mathbf{D}$ , and  $\mathbf{e}_i$  is the  $i^{\text{th}}$  row vector of  $\mathbf{D}$ . The first column/row corresponds to  $\mathcal{P}_{out}$ , the second column/row to  $\mathcal{C}_{in}$ , and so on. We shall iteratively update two sets of scores: (1) raw scores  $\mathbf{S}^{Raw} = [\mathbf{S}_1^{Raw}, \mathbf{S}_2^{Raw}, \mathbf{S}_3^{Raw}, \mathbf{S}_4^{Raw}] = [\mathbf{P}_{out}^{Raw}, \mathbf{C}_{in}^{Raw}, \mathbf{C}_{out}^{Raw}, \mathbf{P}_{in}^{Raw}]$  which are sums of the connection-based rewards and penalties for each vertex; and (2) normalised scores  $\mathbf{S}^{Nrm} = [\mathbf{S}_1^{Nrm}, \mathbf{S}_2^{Nrm}, \mathbf{S}_3^{Nrm}, \mathbf{S}_4^{Nrm}] = [\mathbf{P}_{out}^{Nrm}, \mathbf{C}_{in}^{Nrm}, \mathbf{C}_{out}^{Nrm}, \mathbf{P}_{in}^{Nrm}]$  with

$$\begin{aligned} S_i^{Raw} &= \left(1 - \frac{m}{n^2}\right) \mathbf{A} \mathbf{S}^{Nrm} \mathbf{e}_i^T + \frac{m}{n^2} (1 - \mathbf{A}) \mathbf{S}^{Nrm} (-\mathbf{e}_i^T) \\ &+ \left(1 - \frac{m}{n^2}\right) \mathbf{A}^T \mathbf{S}^{Nrm} \mathbf{d}_i + \frac{m}{n^2} (1 - \mathbf{A}^T) \mathbf{S}^{Nrm} (-\mathbf{d}_i), \end{aligned} \quad (13)$$

for  $i \in \{1, \dots, 4\}$ . The first two terms score the outgoing edge indicators and the last two terms score the incoming edge indicators. The multiplicative constants are chosen to weigh edges in each direction evenly, and to fix the contribution of non-edges to be equal to that of edges.

As the scores in (13) can be negative and the scores for a given vertex may not sum to 1, we normalise as follows. For  $j \in \{1, \dots, n\}$  let  $B(j) = \min\{P_{out}^{Raw}(j), C_{in}^{Raw}(j), C_{out}^{Raw}(j), P_{in}^{Raw}(j)\}$ , and for  $i \in \{1, \dots, 4\}$  we set

$$S_i^{Nrm}(j) = \frac{S_i^{Raw}(j) - B(j)}{\sum_{k=1}^4 (S_k^{Raw}(j) - B(j))}. \quad (14)$$

Thus for each vertex the scores for the four groups sum to 1. If for a given vertex, the raw scores in each of the sets are equal up to floating point error (defined as the denominator of Eq. (14) being less than an arbitrarily fixed constant ( $10^{-10}$ )), we set the normed score in each set to 0.25.



We initialise and update the scores as follows. First, we assign a raw score for each vertex set combination uniformly at random from 0 to 1, which we then use to calculate the normalised scores. We then update each of the scores in turn, first updating  $\mathbf{P}_{out}^{Raw}$  using  $\mathbf{S}^{Nrm}$ , next updating  $\mathbf{S}^{Nrm}$  using the new value of  $\mathbf{S}^{Raw}$ , then repeating the same procedure for each of the remaining scores in the order  $\mathbf{C}_{in}$ ,  $\mathbf{C}_{out}$  and  $\mathbf{P}_{in}$ . We repeat the procedure until convergence, which we measure by computing the largest change observed in each normalised score when we update its raw counterpart; convergence is determined if the largest change over each of the sets is less than  $10^{-8}$ . The general iteration can fail to converge within 1000 iterations. If the scheme has not converged after 1000 steps, we fall back to a scheme which updates the scores on each vertex in turn which often empirically removes the convergence problem with the cost of additional computational complexity. To obtain the set labels, we cluster the normalised score matrix  $\mathbf{S}^{Nrm}$  using k-means++, and allocate each of the clusters to a named set by mapping the clusters to sets which maximises the log-likelihood as will be explained in the next subsection, Section 33.3. We call this method ADVHITS.

The ADVHITS method may lead to large sets having a higher contribution to the score than small sets. Thus, as an alternative scoring system with score matrix  $\mathbf{S}^{Nrm}$ , we introduce a  $4 \times 4$  diagonal matrix  $\mathbf{F}_Y$  with diagonal entries the sum of the scores for the vertices, so that  $(F_Y)_{ii} = 1 / \sum_{j=1}^n S_{ji}^{Nrm}$  for  $i \in \{1, \dots, 4\}$ , and use the iteration scheme

$$\mathbf{S}_i^{Raw} = \mathbf{A} \mathbf{S}^{Nrm} \mathbf{F}_Y \mathbf{e}_i^T + \mathbf{A}^T \mathbf{S}^{Nrm} \mathbf{F}_Y \mathbf{d}_i - \frac{m}{n^2} \mathbf{S}^{Nrm} \mathbf{F}_Y (\mathbf{d}_i + \mathbf{e}_i^T). \quad (15)$$

This iteration scheme makes the contribution from each set to a vertex score identical even for very differently sized sets. The same normalisation scheme and updating scheme as for ADVHITS is then used; we call this method ADVHITSGRP.

### 3.3 Method class 3: Likelihood maximisation

As third method we maximise the likelihood of the directed core–periphery model Eq. (5), which is a stochastic block model with 4 blocks and our particular connection structure. For maximising the likelihood numerically we use, first, a greedy approach from [45] which we call HILLCLIMB, and the second, a slower but potentially more accurate approach from [22] which we call MAXLIKE. HILLCLIMB iteratively updates the values of  $p_1$  and  $p_2$ , and the set assignments. Our implementation deviates slightly from that in [45] for example in having a fixed number of iterations; see SI B. Unlike HILLCLIMB, MAXLIKE does not consider a random order of vertices, but instead updates the vertices in an order which increases the likelihood the most at each step, thus giving a potentially more accurate (albeit slower) algorithm. The complete algorithm can be found in SI B. For multimodal or shallow likelihood surfaces the maximum likelihood algorithms may fail to detect the maximum and instead find a local optimum. Hence we use a range of starting points for the algorithms.

There is a considerable difference in computational cost between HILLCLIMB and MAXLIKE, with one iterate of the HILLCLIMB taking  $O(m)$  time where  $m$  is the number of edges, while for MAXLIKE in sparse networks the computational complexity is  $O(n^2 + m)$ . A detailed discussion around the computational complexity can be found in SI B(c).

## 4 Numerical Experiments on Synthetic Data

To compare the performance of the methods from Section 3, we create three benchmarks using the synthetic model in Section 2 and measure accuracy by computing the Adjusted Rand Index (ARI) [21] between the output partition of a network and the ground truth, using the implementation from [37]. ARI takes values in  $[-1, 1]$ , with 1 indicating a perfect match, and an expected score of approximately 0 under a given model of randomness; a detailed description is given in SI D(a). For completeness, we also compute the similarity using VOI (Variation of Information [34]) and NMI (Normalised Mutual Information [27]), and achieve qualitatively similar results, shown in SI D. As each of our new methods is specifically designed to output the structure in Eq. (4), all of these comparisons can be seen as assessing their performance gain over generic methods in detecting the directed core periphery structure.

We first compare our method against a naïve classifier (DEG.), which performs k-means++ [2] clustering solely on the in- and out-degree of each vertex. To compare against other approaches, we divide our methods into three classes: fast methods (LOWRANK and HITS slow methods (HILLCLIMB and MAXLIKE), and variable methods, namely ADVHITS. We use a separate category for ADVHITS as it can be fast, but in networks with non-existent or weak structure (e.g., Erdős-Rényi random graphs) it can fall back on the single vertex update scheme described at the end of Section 3.2, which reduces the speed considerably. The methods in each of these three classes are compared to methods from the literature that have a similar speed-quality trade-off as the method class it is being compared against.

Our second comparison assesses fast methods against other methods with a similar run time. For completeness, we also compare the ADVHITS method in this comparison. We assess the performance against two well-known fast approaches for directed networks, namely SAPA from [44] and DISUM from [42]. For full details of our implementation and the variants we consider see SI D(e). For brevity we only include the best performing SAPA and DISUM variant namely SAPA2, using degree-discounted symmetrisation, and DISUM3, a combined row and column clustering into four sets, using the concatenation of the left and right singular vectors.

The final comparison assesses full likelihood methods. We compare to the block modelling fitting approach (GRAPHTOOL) from the graph-tool software package [39] based on the approach from [38, 40], by using a procedure that minimises the the minimum description length of the observed data directly. To make this a fair comparison we use the non-degree corrected block modelling fitting approach, and we fix the number of sets at 4, which makes this approach to equivalent to maximising the likelihood. For completeness, we also compare against ADVHITS, as it has a time profile between the fast methods and the slow methods.

**Benchmark 1** We test our approaches using the 1-parameter model from Eq. (6), with equally-sized sets and varying the parameter  $p \in \{0.5, 0.49, 0.48, \dots, 0.21\} \cup \{0.195, 0.19, 0.185, \dots, 0.005\}$ . We choose a finer discretisation step in the  $p$ -range which corresponds to a weaker planted structure, and we average over 50 network samples for each value of  $p$ . Recall that for  $p = 0.5$  the planted structure corresponds to the idealised block structure in Eq. (4) and for  $p = 0$  the planted structure corresponds to an Erdős-Rényi random graph with edge probability 0.5.

The performance results are shown in Table 1, giving the ARI for  $p = 0.4$  and  $p = 0.1$ , and then for values of  $p$  between 0.05 and 0.015 with step size 0.005, in decreasing order.

We graphically compare the performance of 8 of these methods in Figure 2 for  $n = 1000$ , and

$p$ :	0.4	0.1	0.05	0.045	0.04	0.035	0.03	0.025	0.02	0.015
DEG.	1.0	0.985	0.745	0.670	0.592	0.492	0.384	0.279	0.179	0.104
DISUM3	1.0	0.919	0.180	0.115	0.057	0.020	0.007	0.002	0.001	0.000
SAPA2	1.0	0.954	0.186	0.137	0.089	0.044	0.015	0.005	0.002	0.001
HITS	1.0	0.995	0.766	0.687	0.605	0.507	0.393	0.255	0.160	0.094
LOWRANK	1.0	0.992	0.764	0.687	0.605	0.506	0.393	0.255	0.160	0.094
ADVHITS	1.0	1.0	0.888	0.825	0.733	0.613	0.479	0.335	0.196	0.103
GRAPHTOOL	1.0	1.0	0.965	0.928	0.797	0.013	0	0	0	0
HILLCLIMB	1.0	1.0	0.967	0.932	0.874	0.763	0.611	0.412	0.216	0.096
MAXLIKE	1.0	1.0	0.967	0.932	0.874	0.751	0.611	0.409	0.215	0.093

Table 1: ARI of the methods under comparison on Benchmark 1 for different values of  $p$  and with network size  $n = 1000$ .

we further present a comparison with the case where  $n = 400$  in SI D(b). For ease of readability HILLCLIMB is not included in Figure 2 as Table 1 illustrates that its performance is very similar to MAXLIKE.

We observe that in all cases, Method class 3 (likelihood maximisation) outperforms the other approaches for a large range of  $p$ . The ADVHITS algorithm also achieves good performance, while taking less run time than the likelihood approaches (see SI D(c) for further details on run time). For NMI and VOI we observe similar qualitative results, see SI D.

Above a certain threshold of  $p$  (roughly around  $p = 0.2$ ), many approaches including the degree-based approach DEG. achieve optimal performance, indicating that in this region of the networks obtained with Benchmark 1, the degrees alone are sufficient to uncover the structure. Below this threshold, the ADVHITS and likelihood approaches strongly outperform the degree-based approach, while the LOWRANK and HITS methods equal the performance of the degree method in some regions and outperform it in others.

SAPA2 from [44] and DISUM3 from [42] are outperformed by our methods LOWRANK, HITS, and ADVHITS. The slow likelihood-based methods MAXLIKE and HILLCLIMB outperform even GRAPHTOOL which fits a general block model to the data, although the difference is less pronounced than the difference between the fast methods. Finally, we note that the performance of GRAPHTOOL collapses as  $p$  gets close to 0 (similar behaviour is observed for  $n = 400$  see SI D(b)). Further investigation indicated that for low values of  $p$ , GRAPHTOOL often places most vertices in a single set (see SI D for further details).

**Benchmark 2** We use the two-parameter model from Eq. (5), again with all four sets of the same size  $\frac{n}{4}$ , now the edge probabilities  $(p_1, p_2)$  vary the density and the strength of the core periphery structure. To this end, we vary  $p_1$ , and the ratio  $0 \leq \frac{p_2}{p_1} < 1$ . For a given  $p_1$ ,  $\frac{p_2}{p_1} = 0$  corresponds to the strongest structure and  $\frac{p_2}{p_1} = 1$  to the weakest structure. We generate 10 networks each with  $p_1 \in \{0.025, 0.05, \dots, 1.0\}$  and  $\frac{p_2}{p_1} \in \{0, 0.05, \dots, 0.95\}$ , resulting in 820 parameter instances of  $(p_1, \frac{p_2}{p_1})$ . The results for  $n = 1000$  are in Fig. 3 with a comparison to  $n = 400$  presented in SI D(b). We present the contours corresponding to an average ARI of 0.75. Due to space constraints, we only display HITS, LOWRANK, ADVHITS and MAXLIKE as well as the best-performing other methods SAPA2, GRAPHTOOL and DEG. The performance of HILLCLIMB is again very similar to that of

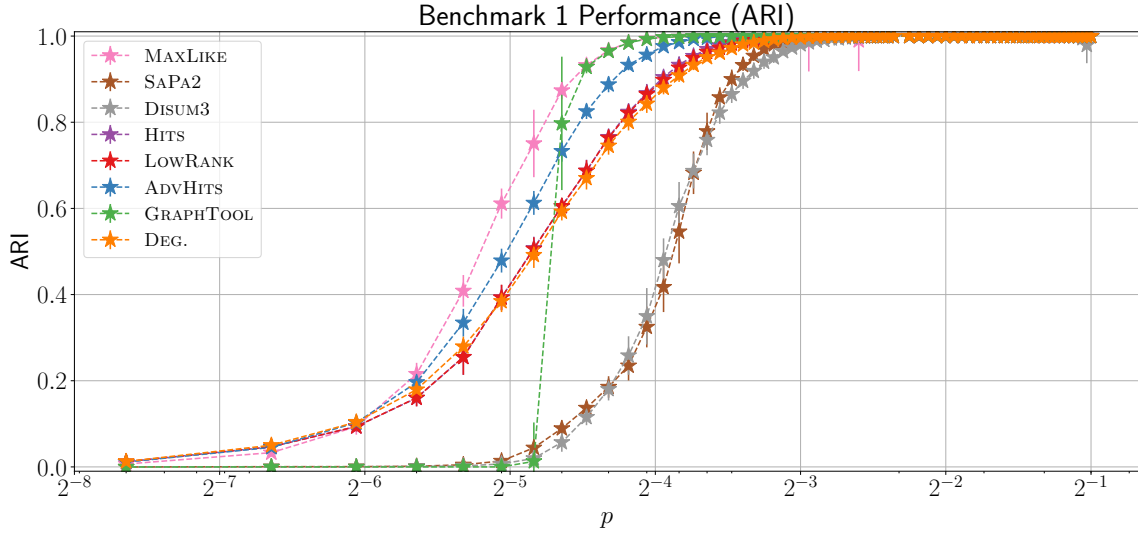


Figure 2: Performance on Benchmark 1 (see Eq. (6)). The ARI between the planted partition of the graph and the partition detected by each method for networks of size  $n = 1000$ . On the  $x$  axis, we vary the parameter  $p$  on a log scale. Error bars are one sample standard deviation.

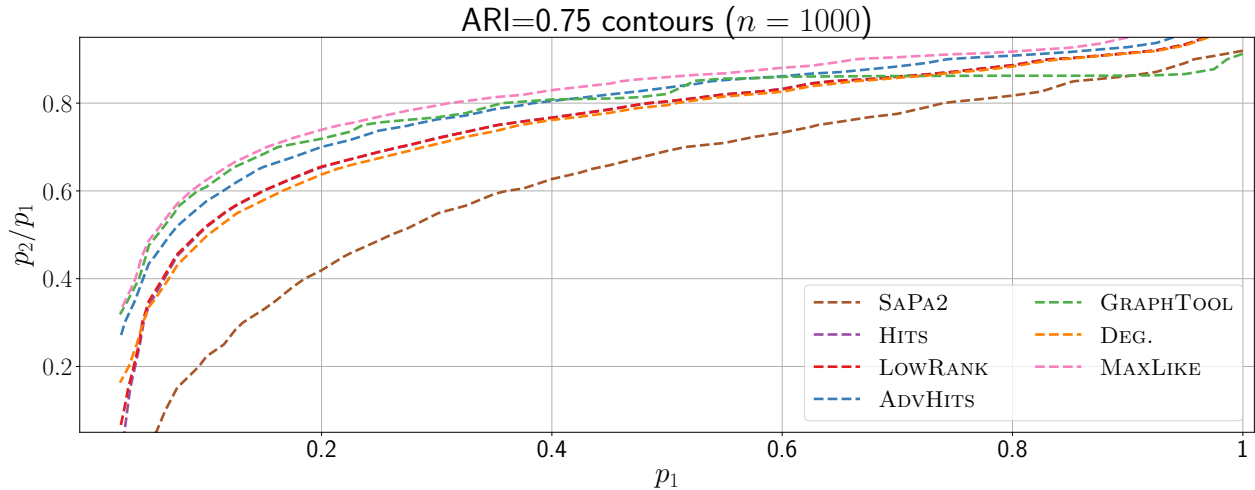


Figure 3: Contour plot of  $\text{ARI}=0.75$  on Benchmark 2 (see Eq. (5)). For this plot, we calculate the average ARI over 10 networks of size  $n = 1000$  varying  $p_1 \in \{0.025, 0.05, \dots, 1.0\}$  and  $\frac{p_2}{p_1} \in \{0, 0.05, 0.1, \dots, 0.95\}$ , and then display the contours corresponding to an average ARI of 0.75. We note that the fast methods HITS and LOWRANK outperform the comparisons DEG. and SAPA2, although they are hard to distinguish due to similar performance.

MAXLIKE and not shown. The same comparisons performed using VOI and NMI can be found in SI D.

As observed for Benchmark 1, the full likelihood approaches outperform all other methods, with the performance of ADVHITS coming close and outperforming GRAPHTOOL in certain regions. Comparing the fast methods only, again, the slower ADVHITS approach outperforms all of the other fast approaches, performing almost as well as the full likelihood MAXLIKE method. Within the slow methods, MAXLIKE outperforms GRAPHTOOL, although occasionally it only finds a local maximum.

The 0.9 contour ( Fig. SI 2 of SI D) shows that the performance of GRAPHTOOL is closer to that of the likelihood methods compared to the 0.75 contour. This could again be related to GRAPHTOOL often placing all vertices in the same community when the structure is weak.

**Benchmark 3** Benchmark 3 assesses the sensitivity of our methods to different set sizes. In the 1-parameter model from Eq. (6), fix  $p = 0.1$  as this value is sufficiently large to see variation in performance between our approaches, but sufficiently small that most of the methods can detect the underlying structure. We then fix the size of three of the sets and vary the size of the final set. For example, to vary  $\mathcal{P}_{out}$ , we fix  $n_{\mathcal{C}_{in}} = n_{\mathcal{C}_{out}} = n_{\mathcal{P}_{in}} = \frac{n}{4}$  and test performance when we let  $n_{\mathcal{P}_{out}} \in \{2^{-3\frac{n}{4}}, 2^{-2\frac{n}{4}}, \dots, 2^{3\frac{n}{4}}\}$ , with equivalent formulations for the other sets.

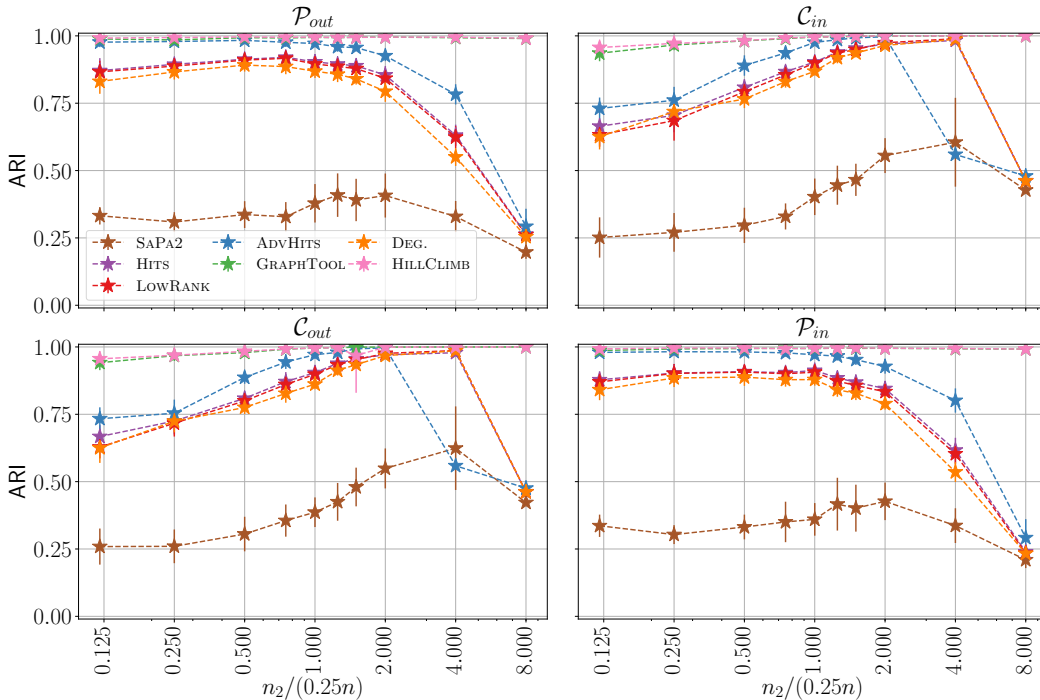


Figure 4: ARI of all methods on Benchmark 3 with sets of different sizes (see Eq. (5)). We fix  $p = 0.1$ , the size of 3 sets at  $n/4$  with  $n = 400$ , and vary the size (denoted as  $n_2$ ) of the fourth set. Error bars are one sample standard deviation.

Results for  $n = 400$  are shown in Fig. 4. The relative performance of the methods matches that of the first two synthetic experiments, with the likelihood methods performing best, followed by ADVHITS, then by the faster LOWRANK and HITS methods, and finally by the other spectral

approaches. The likelihood methods appear to be robust to set size changes. The performance of the faster methods depends on core or periphery set changes. In the periphery, smaller set sizes seem to have a minimal impact on performance, while large set sizes lead to a large decay in performance. In the core, both smaller and larger sets appear to have a significant impact. For a large core set, the fast methods outperform the ADVHITS methods, as the performance of ADVHITS decays much faster, and in some cases, ADVHITS is even outperformed by DEG.

## 5 Application to real world data

Next, we test our methods on three real-world data sets, namely Political Blogs (*Blogs*) from [1] (Section 55.1), Faculty hiring data (*Faculty*) from [11] (Section 55.2), and Trade data (*Trade*) from [17] (Section 55.3). In each case our methods find a division into four sets and we explore the identified structure using any known underlying attributes. For each data set, we first assess the consistency of the partitions both within and between each of the approaches. We compute 11 runs for each of the fast methods, 1 run for the slow methods, and then compute the within-method ARI between the resultant partitions and the ARI between methods of different types. We also compare with the structure uncovered by bow-tie [10], as discussed in Section 1. Bow-tie can allocate vertices to several sets – there is a core set, an incoming periphery set, an outgoing periphery set and 4 additional sets corresponding to other connection patterns. Thus, we consider the ARI between the partition into 7 sets (BOWTIE), and the partition induced only by the core set and the in- and out-periphery sets (BOWTIEADJ). When computing the ARI between the partition induced by the core and periphery sets of BOWTIE (the partition we call BOWTIEADJ) with another partition  $\mathcal{S}$ , we consider the partition induced by  $\mathcal{S}$  on the vertex-set in BOWTIEADJ (and thus, by construction, the ARI between BOWTIEADJ and BOWTIE is always 1).

As there is no “ground truth” core-periphery structure available for these networks, we carry out a Monte Carlo test to assess whether the detected structure could plausibly be explained as arising from random chance. To this end, we take the difference between the probability of connection within the ‘L’ shape ( $d_{in}$ ), with that outside of the ‘L’ shape ( $d_{out}$ ), maximising the likelihood over the  $4! = 24$  ways of rearranging the sets. This statistic is used in two Monte Carlo tests, with 250 repeats each, against the following null models: (1) a directed Erdős-Rényi (ER) model without self-loops (using the standard NetworkX implementation [19]) in which we set the number of vertices and the connection probability equal to those of the observed network, and (2), inspired in part by [4], a directed configuration model with self-loops (again using the standard NetworkX implementation [19]), which adjusts for the in- and out-degree of the vertices, collapsing multi-edges into a single edges. In ADVHITS, these Monte Carlo tests often fall back to the single vertex update scheme and thus can be slow.

### 5.1 Political Blogs

The data set, *PolBlogs* from [1] consists of political blogs as vertices, and directed edges from one Blog to another denoting that the first blog contains at least one link to the second blog. The data set was collected on a single day during the 2004 US presidential election. After collapsing 65 multi-edges, it contains 1490 vertices and 19090 edges. The set of blogs is divided into 758 liberal blogs and 732 conservative blogs. For the analysis in this section, we focus on the largest weakly connected component of the network, which has  $n = 1222$  vertices and 19024 edges.

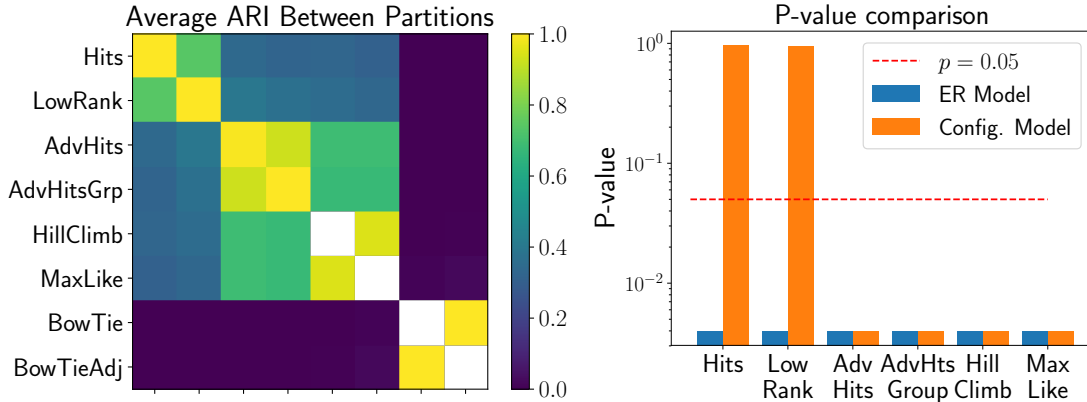


Figure 5: *PolBlog* results **Left panel** The ARI between the partitions uncovered by each method. For ease of comparison, negative values are set to 0. For the faster methods we compare with 11 runs and show the average similarity between all pairs of partitions whereas for the slow methods, we use a single run and thus display a blank (white) square on the corresponding diagonal blocks. To compare to bow-tie, we compare both to the partition into 7 sets and a partition formed by a subset of the vertices corresponding to the main three sets. **Right panel** The  $p$ -values of the Monte Carlo test on each partition against a directed ER and a directed configuration model.

The first panel of Fig. 5 shows the ARI between the different approaches. We note a high within-method ARI, and a high ARI between HITS and LOWRANK (perhaps unsurprisingly, as both use centrality-based scores), and also a high ARI between ADVHITS and ADVHITSGRP and between the likelihood methods. Furthermore, there is a low ARI between our methods and bow-tie, indicating that our methods uncover a different structure.

The Monte Carlo  $p$ -values of the tests described at the beginning of this Section can be seen in Fig. 5. The HITS and LOWRANK methods are significant at 5% level against the directed ER null model but not against the directed configuration model, potentially indicating that the structures found are a function of the in- and out-degree distribution. It is of course possible that LOWRANK and HITS uncover significantly non-random structures, just that these structures do not correspond to an ‘L’-shape structure. The other structures are significant at a 5% level on both tests. Noting the similarity between the likelihood methods, for brevity we restrict our discussion to ADVHITS method and MAXLIKE.

Beginning with the ADVHITS method, Fig. 6 presents both a network visualisation and a matrix showing the density of edges between each pair of sets. The underlying density structure reveals an ‘L’-shape, albeit a weaker connection than anticipated in  $\mathcal{P}_{in}$ .

Assessing whether the partitions which are found by ADVHITS and MAXLIKE methods relate to the classification of a blog as liberal or conservative, we observe that the partitions are not just a function of political affiliation; see Fig. SI 9 in SI E for full details. Instead, similar to the division in [52], the sets may relate to the role they play in the network. Indeed, the in- and out-degree distributions in each of the sets, as shown in Fig. 7A, indicate that the sets  $\mathcal{P}_{out}$ ,  $\mathcal{C}_{in}$  and  $\mathcal{C}_{out}$  have in- and out-degrees which correspond to a core-periphery structure.

Directly comparing the ADVHITS partition with the core-periphery partition, using the stochastic block model approach from [52], as implemented in the cpalgorithm package [25], we uncover

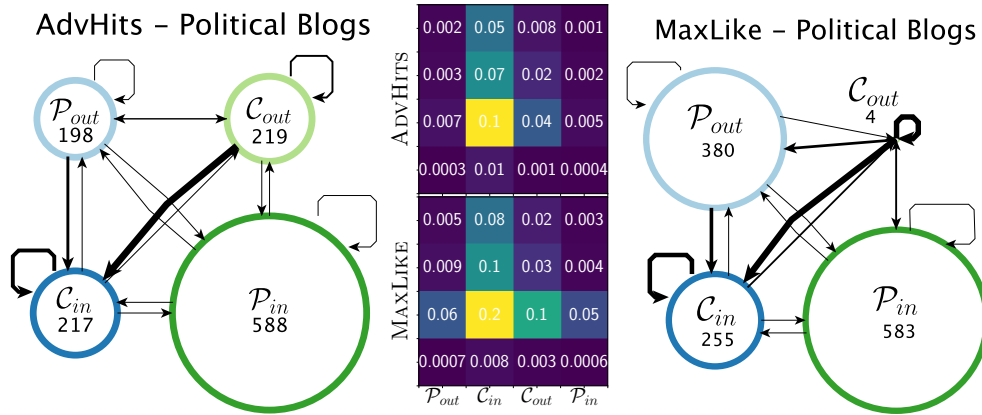


Figure 6: Structures in *PolBlogs*. In the **left** (ADVHITS) and **right** (MAXLIKE) panels, we show summary network diagrams associated with the uncovered structures. In these summaries the size of each of the vertices is proportional to the number of vertices in each set, and the width of the lines is the percentage of edges that are present between the sets. The width of lines is designed to highlight the differences and is not comparable between plots. The centre panel displays the percentage of edges between each pair of blocks, allowing for easy visualisation of the ‘L’-structure.

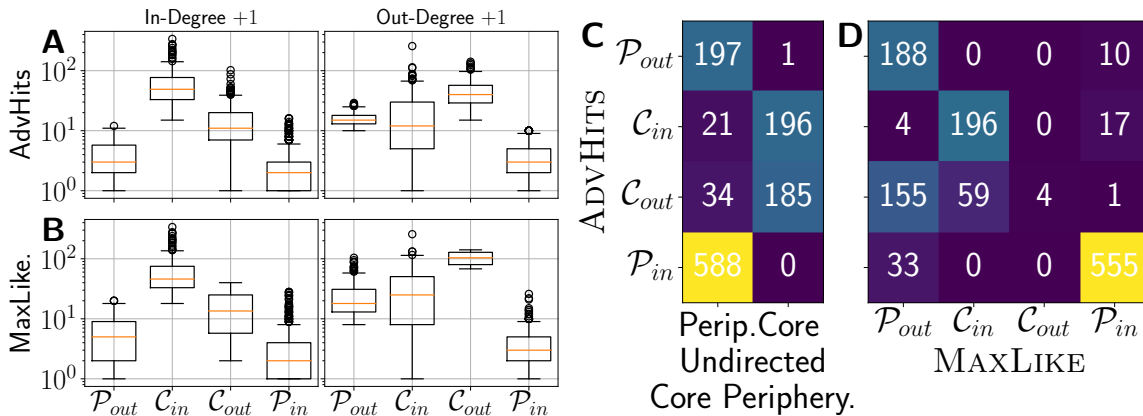


Figure 7: **A** - Boxplot of in- and out-degree in each of the sets in ADVHITS. **B** - Boxplot of in- and out-degrees in each of the sets in MAXLIKE. To visualise the in- and out-degrees on a log scale, we add 1 to the degrees. **C** - Confusion table between the ADVHITS partition and the division into a standard core-periphery structure. **D** - Confusion table between the partition given by ADVHITS and the partition by MAXLIKE.



the confusion table in Fig. 7C. Our method splits the previously detected core into two distinct sets which fulfil different roles, and to a lesser extent, splits the periphery in a similar way. In the case of the periphery sets, this could be the propensity of the individual site owners to link out to other content, as both periphery sets have a similar average in-degree, but differ on out-degree, a property controlled by the authors of the blog.

A possible explanation for the split within the cores is that the  $\mathcal{C}_{in}$  set represents blogs that are seen as authorities, and thus do not link to many other blogs (but are linked to themselves), whereas the opposite is true of those in  $\mathcal{C}_{out}$ . A potentially related structure was observed in 15-block SBM from [40], in which they identify blocks that cite but are not cited, and other blocks which are highly cited either in general or by specific groups. To assess this hypothesis, an inspection of the web-address corresponding to the vertices in each set suggests that certain sets are enriched for ‘blogspot’ sites. A ‘blogspot’ site is a free blogging site that requires less expertise to set up than a full website. Indeed, while the fractions of ‘blogspot’ sites in  $\mathcal{P}_{out}$  (0.566),  $\mathcal{C}_{out}$  (0.411), and  $\mathcal{P}_{in}$  (0.454) are relatively similar, the percentage in  $\mathcal{C}_{in}$  is distinctly smaller at 0.180, supporting our hypothesis. Moreover, [1] provides a list of the top 20 conservative and the top 20 liberal blogs, by filtering the top  $\approx 100$  liberal and conservative blogs by degree, and ranking the top blogs by the number of citations of blog posts in an external index (see [1] for details). In ADVHITS, 100% of these top blogs are in  $\mathcal{C}_{in}$ , again supporting our hypothesis.

The structure uncovered with MAXLIKE, shown in Fig. 6 again has an ‘L’-shape structure, indicating a split into the 4 roles; compared to ADVHITS, the size of  $\mathcal{C}_{out}$  is greatly reduced with a much larger  $\mathcal{P}_{out}$  and a slightly enlarged  $\mathcal{C}_{in}$ . We first note that the likelihood of this structure is higher than that of the ADVHITS method. The confusion table between this structure and the ADVHITS structure in Fig. 7D suggests that most of the vertices in  $\mathcal{C}_{out}$  in the ADVHITS structure have moved to  $\mathcal{P}_{out}$ , with a reasonably sized subset also moving to  $\mathcal{C}_{in}$ . The confusion table has a small number of large values, indicating that many pairs of vertices in the same set in one partition are also in the same set in the other. This is consistent with our previous assertion that the partitions are similar (as measured by ARI). The degree patterns of each of the sets are still preserved, see Fig. 7B, although with a much larger out-degree in  $\mathcal{C}_{out}$ . This split indicates a different partition of the sets into a large out-linking set consisting of 4 vertices with large out-degree, with the remaining vertices mostly moving to  $\mathcal{P}_{out}$ . Furthermore, while the undirected core–periphery structure is not visible here (see Fig. SI 10 in SI E), the confusion table indicates that the  $\mathcal{C}_{in}$  set is relatively unchanged,. The ‘blogspot’ statistic (0.21 in  $\mathcal{C}_{in}$  versus  $> 0.43$  in all other sets) and 39 out of 40 top blogs are in  $\mathcal{C}_{in}$  in this division, also support the interpretation that  $\mathcal{C}_{in}$  is enriched for authorities.

## 5.2 Faculty Hiring

In the faculty hiring network from [11], vertices are academic institutions, and a directed edge from institution  $i$  to  $j$  indicates that an academic received their PhD at  $i$  and then became faculty at  $j$ . The data set is divided by gender, faculty position, and into three fields (Business, Computer Science, and History). For brevity, we only consider the overall connection pattern in Computer Science. In [11] it is found that a large percentage of the faculty is trained by a small number of institutions, and it is suggested that there exists a core–periphery-like structure.

We apply our methodology to this data set, and find that the results from the ADVHITS variants and the likelihood methods are significant at 5% under both random null models. The partitions within method class are again very similar (data not shown). For brevity, due to the similarity

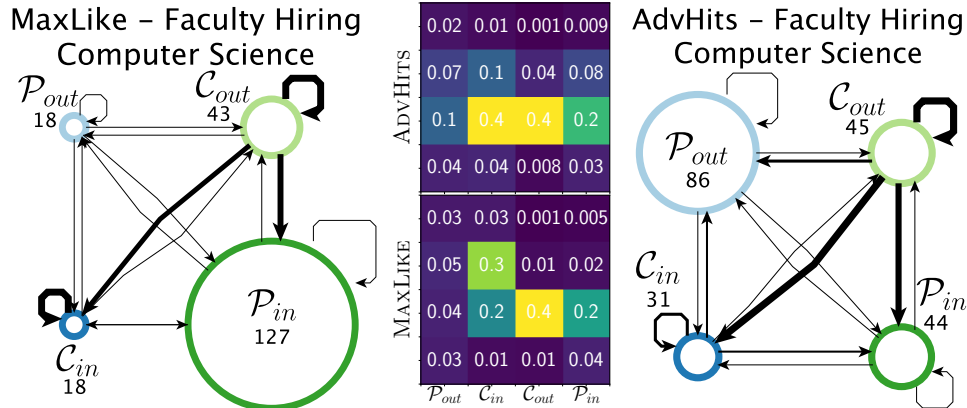


Figure 8: Structures in *Faculty* uncovered by MAXLIKE and the ADVHITS. In the **left** (MAXLIKE) and **right** (ADVHITS) panels we show summary network diagrams associated with the uncovered structures. In these summaries the size of each of the vertices is proportional to the number of vertices in each set, the width of the lines is given by the percentage of edges that are present between the sets. The width of lines is designed to highlight the differences and is therefore not comparable between plots. The centre panel displays the percentage of edges between each pair of blocks which allowing easily visualisation of the ‘L’-structure.

between the partitions, we focus on the results from the MAXLIKE and ADVHITS.

The MAXLIKE results in Fig. 8 show a clear ‘L’-shape structure, albeit with a weakly defined  $\mathcal{P}_{out}$ . Inspecting the sets,  $\mathcal{C}_{out}$  consists of highly-ranked institutions, including Harvard, Stanford, MIT and also a vertex that represents institutions outside of the data set. Fig. 9C shows the University ranking  $\pi$  obtained by [11], and the two other University rankings used in the [11], abbreviated NRC95 and USN2010, in each of the sets which are found using MAXLIKE. Here, the NRC95 ranking from 1995 was used because the computer science community rejected the 2010 NRC ranking for computer science as inaccurate. The NRC ranked only a subset of the institutions; all other institutions were assigned the highest NRC rank  $+1 = 92$ . The set  $\mathcal{C}_{out}$  has considerably smaller ranks than the other sets, indicating that  $\mathcal{C}_{out}$  is enriched for highly ranked institutions. The set  $\mathcal{P}_{in}$  from MAXLIKE appears to represent a second tier of institutions who take academics from the schools in  $\mathcal{C}_{out}$  (Fig. 8) but do not return them to the job market. This observation can again be validated by considering the rankings in [11] (Fig. 9C). The  $\mathcal{C}_{in}$  set loosely fits the expected structure with a strong incoming link from  $\mathcal{C}_{out}$  and a strong internal connection (Fig. 8), suggesting a different role to that of the institutions in  $\mathcal{P}_{in}$ . A visual inspection of the vertices in  $\mathcal{C}_{in}$  reveals that 100% of the institutions in  $\mathcal{C}_{in}$  are Canadian (also explaining the lack of ranking in USN2010 (Fig. 9C)). In contrast, the proportion of Canadian universities in  $\mathcal{P}_{out}$  is 11.1%; in  $\mathcal{C}_{out}$  it is 2.3%, and in  $\mathcal{P}_{in}$  it is 0.79%. This finding suggests that Canadian universities tend to play a structurally different role to US universities, tending to recruit faculty from other Canadian universities, as well as from the top US schools. In [11] the insularity of Canada was already noted, but without a core-periphery interpretation.

Finally,  $\mathcal{P}_{out}$  is weakly connected both internally and to the remainder of the network (Fig. 8). In each of the rankings (Fig. 9C),  $\mathcal{P}_{out}$  has slightly lower average ranks than the other sets (with the exception  $\mathcal{C}_{in}$ , due to the default/missing rankings of Canadian institutions). This could indicate

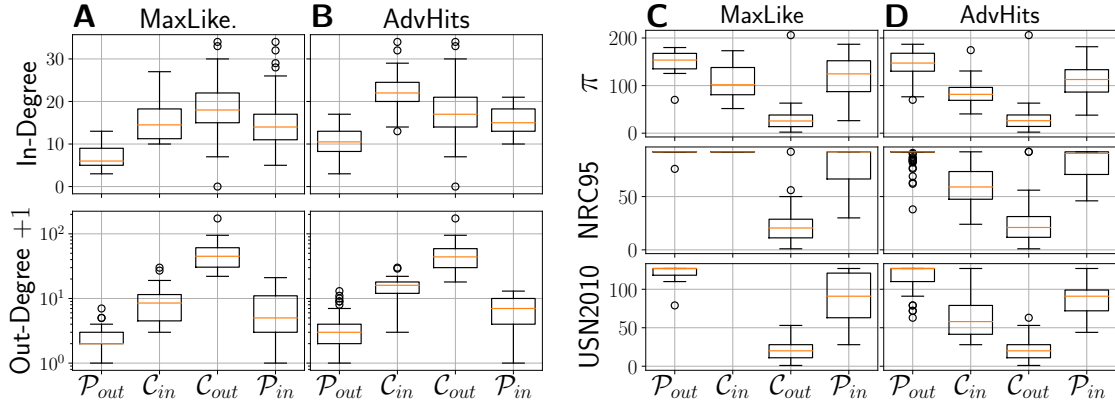


Figure 9: **A** - Boxplot of in- and out-degrees in each of the sets in MAXLIKE. **B** - Boxplot of in- and out-degrees in each of the sets in ADVHITS. To visualise the out-degrees on a log scale, we add 1 to the degrees. **C** - Boxplot of the ranking in [11], denoted  $\pi$ , ranking in NRC95 and the ranking in USN2010 in each of the sets in MAXLIKE. **D** - Boxplot of the ranking in [11], the ranking in NRC95 and the ranking in USN2010 in each of the sets in ADVHITS.

that  $\mathcal{P}_{out}$  consists of lower ranked institutions which are not strong enough to attract faculty from the larger set of institutions. The in- and out-degree distributions, (Fig. 9A), show that  $\mathcal{P}_{out}$  has lower in and out-degree distributions than the other sets. Thus, an alternative hypothesis is that  $\mathcal{P}_{out}$  consists of universities with smaller Computer Science departments which do not interact with the wider network. We leave addressing this interpretation to future work. In either case, the institutions in  $\mathcal{P}_{out}$  do not appear to match the pattern observed in the remainder of the network and hence it is plausible to delegate them into one set.

While in the ADVHITS result (Fig. 8),  $\mathcal{C}_{out}$  plays the same role as in the MAXLIKE partition, with an overlap of 42 vertices out of sets of size 43 and 45, the remaining sets appear to have a different structure. The distribution of in- and out-degrees, shown in Fig. 9B, indicates that the out-degrees of the sets tend to be much smaller than the sets uncovered by MAXLIKE. Further, unlike in the MAXLIKE case, there is a stronger ordering with respect to the academic performance of the sets (Fig. 9D). This suggests that  $\mathcal{C}_{in}$  could represent a second tier of institutions which take faculty members from  $\mathcal{C}_{out}$  but also take faculty members from within (the density of self-loops in  $\mathcal{C}_{in}$  is 0.11, in contrast to 0.011 in  $\mathcal{P}_{out}$  and 0.039 in  $\mathcal{P}_{in}$ ),  $\mathcal{P}_{in}$  may represent a third tier of institutions which contains institutions that attract a large number of academics from  $\mathcal{C}_{out}$ , while  $\mathcal{P}_{out}$  may represent a fourth tier set which contains institutions that do not tend to take academics from the highest-ranked universities.

### 5.3 World Trade data

The World Trade data set from [17] has countries as vertices and directed edges between countries representing trade. For simplicity, we focus on data from 2000 and restrict our attention to the trade in fresh, chilled and frozen bovine meats. We remove trades that do not correspond to a specific country, resulting in 720 trades for bovine meats involving 125 countries, which leads to a network density of roughly 0.046.

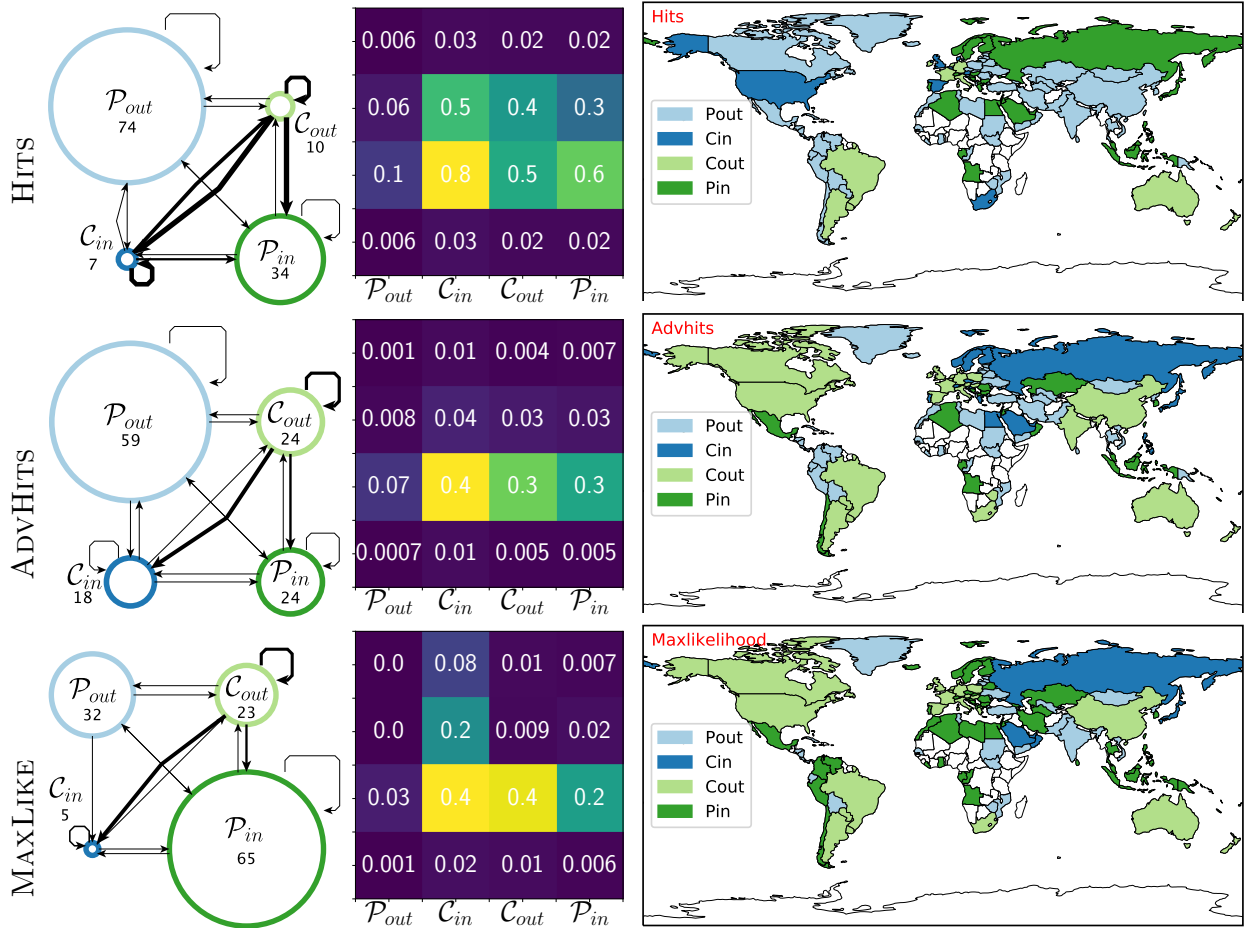


Figure 10: Structures in *WorldTrade*. In the **top** (HITS), **middle** (ADVHITS) and **bottom** (MAXLIKE) panels we show summary network diagrams associated with the uncovered structures. In these summaries the size of each of the vertices is proportional to the number of vertices in each set, the width of the lines is given by the percentage of edges that are present between the sets. The width of lines is designed to highlight the differences and is therefore not comparable between plots. The centre panel displays the percentage of edges between each pair of blocks which allowing easily visualisation of the ‘L’-structure. The right panel visualises the partition on a World map.

The ARIs of the partitions again show high similarity within method class (data not shown). All methods except LOWRANK show significant deviation from random when compared to the directed ER and directed configuration models. First, we focus on the partition uncovered by HITS shown in Fig. 10. The structure does not have a clearly visible ‘L’-shape structure, but in HITS the internal ‘L’ density is sufficiently high to pass the significance tests. Inspecting the sets,  $\mathcal{C}_{out}$  has high out-degree and often low in-degree vertices, which corresponds to large beef exporting nations, including Argentina, Australia, and Brazil. The set  $\mathcal{C}_{in}$  corresponds to nations that import and export, with strong imports from the  $\mathcal{C}_{out}$  set, including the UK and South Africa, whereas  $\mathcal{P}_{in}$  countries are primarily importers with many vertices with out-degree 0, including Russia which strongly imports from  $\mathcal{C}_{out}$ . Finally,  $\mathcal{P}_{out}$  corresponds to mostly low degree vertices.

ADVHITS yields a different partition, producing a weak ‘L’-shape structure. The  $\mathcal{C}_{in}$  and  $\mathcal{C}_{out}$  sets from the HITS division being combined with additional vertices to form the ADVHITS’  $\mathcal{C}_{out}$  set, resulting in a set with large out-degrees and a range of in-degrees. The sets  $\mathcal{P}_{in}$  and  $\mathcal{C}_{in}$  then are enriched for countries with strong imports from the  $\mathcal{C}_{out}$  countries, with  $\mathcal{C}_{in}$  having a larger average in-degree (and the set with the largest out-degree after  $\mathcal{C}_{out}$ ), and  $\mathcal{P}_{out}$  countries have on average a low in- and out-degree. This structure is close to a classic core–periphery structure, with one core having a high out-degree linking to a large number of peripheral countries.

Finally, MAXLIKE obtains a full ‘L’ structure; Fig. 10 shows that the geographic distribution is similar to the structure from ADVHITS. There is a strong overlap between their respective  $\mathcal{C}_{out}$  sets (22 shared vertices), indicating that it finds a similar core to the ADVHITS. Similarly,  $\mathcal{C}_{in}$  is a subset of ADVHITS’s  $\mathcal{C}_{in}$  (overlap 4), but in MAXLIKE this focuses on a small set of heavily importing countries with a large in-degree and a small out-degree, which includes Japan, Oman, Russia, Saudi Arabia and United Arab Emirates. The connection pattern clearly indicates this is a set which behaves differently from the others, and we leave further investigation as future work. The periphery division is also different;  $\mathcal{P}_{in}$  consists of countries with a large number of imports from  $\mathcal{C}_{out}$ . In  $\mathcal{P}_{out}$ , there are certain vertices with an expected structure, e.g. Ukraine, Mongolia, Lithuania and Moldova supplying Russia ( $\mathcal{C}_{in}$ ) and Pakistan, India and Sudan which supply the Arabian Peninsula. However, there are a number of vertices that do not match the pattern and may just be low degree vertices that are difficult to place.

Overall, in our final real-world data set, we demonstrated the power of our method, uncovering three related but different core-periphery structures: a two-core structure from HITS, a single-core structure from ADVHITS, and a two-core, two-periphery structure from MAXLIKE.

## 6 Conclusion and further work

We provide the first comprehensive treatment of a directed discrete core–periphery structure which is not a simple extension of bow-tie structure. The structure we introduced consists of two core sets and two periphery sets defined in an edge-direction-dependent way, each with a unique connection profile. To detect this structure algorithmically, we proposed three method classes with different speed-quality trade-offs. The fastest algorithms exploit the low-rank structure of the network and cluster the corrected degrees using k-means++, the slower set of algorithms use an iterative scheme based on the connection structure and are inspired by the HITS algorithm, and the slowest but most accurate approaches directly maximise a likelihood function.

Using our synthetic model for this novel directed core–periphery structure, we created three benchmarks, to compare our specialised approaches to four directed network clustering methods

that have similar speed-quality trade-offs. We found that all of our proposed approaches match or outperform clustering solely using the in- and out-degrees. Furthermore, our fast methods outperform the fast spectral comparisons from the literature, and similarly, our slow methods outperform existing slow methods. As our methods are tailored to detect the planted directed core-periphery structure, this finding is reassuring but not surprising.

Then we explored the existence of our directed core-periphery structure in three real-world data sets, namely a political blog network, a faculty hiring network, and a world trade network. In each data set, we found at least one significant structure, when compared to random ER and configuration model graphs. In the political blogs data set, our ADVHITS method, revealed a division of the classically discovered core into two independent components, a  $\mathcal{C}_{in}$  core which we hypothesise consists of authorities which are highly referenced, and a  $\mathcal{C}_{out}$  core which link to a large number of other blogs. We support this hypothesis by noting that  $\mathcal{C}_{in}$  has a much lower percentage of ‘blogspot’ sites than the other set, and that  $\mathcal{C}_{in}$  contains all of the top blogs identified by [1]. In the faculty hiring data set, the MAXLIKE partition uncovers a new structure, namely Canadian universities which have a large number of links with the top US schools, but also appear to strongly recruit from their own schools, indicating a complementary structure to the one found in [11]. In the trade data, we found different but related core-periphery structures using each of our methods. With HITS we obtained a two-core structure which highlights strong exporters as well as those who both import and export; with ADVHITS we obtain a structure which is closer to a classical core-periphery structure, and finally with MAXLIKE we obtain two cores related to strong exporters and a surprising set of strong importers, a well defined  $\mathcal{P}_{in}$  set, and a less well defined but coherent  $\mathcal{P}_{out}$  set.

Here are some avenues for future work. The trade data highlighted that some vertices simply may not fit the core-periphery pattern, and thus following the formulation of bow-tie, it would be interesting to explore modifications to our approaches that would allow us not to place vertices if they do not match the pattern (for example, by introducing a separate set for outlier vertices). Further future work would explore graph regularisation techniques which may increase performance for sparse networks.

Moreover, as detailed in SI A, other directed core-periphery patterns are possible. Some of our methods could be adapted to also detect such core-periphery patterns. In principle, all possible core-periphery structures could be tested simultaneously, with an appropriate correction for multiple testing. Such a development should of course be motivated by a suitable data set which allows for interpretation of the results. More generally, meso-scale structures may change over time, and it would be fruitful to extend our structure and methods to include time series of networks.

**Acknowledgements** This work was funded by EPSRC grant EP/N510129/1 at The Alan Turing Institute and Accenture Plc. In addition, we acknowledge support from COST Action CA15109. We thank Aaron Clauset for useful discussions and the authors of [49] for providing the code for the bow-tie structure.

## References

- [1] Lada A Adamic and Natalie Glance. The political blogosphere and the 2004 us election: divided they blog. In *Proc. of the 3rd international workshop on Link discovery*, pages 36–43. ACM, 2005.

- [2] David Arthur and Sergei Vassilvitskii. k-means++: the advantages of careful seeding. In *SODA '07: Proceedings of the eighteenth annual ACM-SIAM symposium on Discrete algorithms*, pages 1027–1035. Society for Industrial and Applied Mathematics, 2007.
- [3] N. Azimi-Tafreshi, S. N. Dorogovtsev, and J. F. F. Mendes. Core organization of directed complex networks. *Phys. Rev. E*, 87:032815, Mar 2013.
- [4] Paolo Barucca and Fabrizio Lillo. Disentangling bipartite and core-periphery structure in financial networks. *Chaos Soliton Fract*, 88:244 – 253, 2016.
- [5] Mariano Beguerisse-Díaz, Guillermo Garduno-Hernández, Borislav Vangelov, Sophia N Yaliraki, and Mauricio Barahona. Interest communities and flow roles in directed networks: the twitter network of the uk riots. *J. Royal Soc. Interface*, 11(101):20140940, 2014.
- [6] Carl Friedrich Bolz, Antonio Cuni, Maciej Fijalkowski, and Armin Rigo. Tracing the meta-level: Pypy’s tracing jit compiler. In *Proc. of the 4th Workshop on the Implementation, Compilation, Optimization of Object-Oriented Languages and Programming Systems*, ICPOOLPS '09, pages 18–25, NY, USA, 2009. ACM.
- [7] Stephen P. Borgatti and Martin G. Everett. Models of core/periphery structures. *Soc. Netw.*, 21:375–395, 1999.
- [8] A. Borodin, G. O. Robert, J. S. Rosenthal, and P. Tsaparas. Link analysis ranking: Algorithms, theory, and experiments. *ACM Transactions on Internet Technology*, 2005.
- [9] John P. Boyd, William J. Fitzgerald, Matthew C. Mahutga, and David A. Smith. Computing continuous core/periphery structures for social relations data with minres/svd. *Soc. Netw.*, 32(2):125 – 137, 2010.
- [10] Andrei Broder, Ravi Kumar, Farzin Maghoul, Prabhakar Raghavan, Sridhar Rajagopalan, Raymie Stata, Andrew Tomkins, and Janet Wiener. Graph structure in the web. *Comput. Netw.*, pages 309–320, 2000.
- [11] Aaron Clauset, Samuel Arbesman, and Daniel B Larremore. Systematic inequality and hierarchy in faculty hiring networks. *Sci. Adv.*, 1(1):e1400005, 2015.
- [12] Thomas M. Cover and Joy A. Thomas. *Elements of Information Theory (Wiley Series in Telecommunications and Signal Processing)*. Wiley-Interscience, New York, NY, USA, 2006.
- [13] Peter Csermely, András London, Ling-Yun Wu, and Brian Uzzi. Structure and dynamics of core/periphery networks. *J. Complex Netw.*, 1(2):93–123, 2013.
- [14] Mihai Cucuringu, Ioannis Koutis, Sanjay Chawla, Gary L. Miller, and Richard Peng. Simple and Scalable Constrained Clustering: a Generalized Spectral Method. *AISTATS 2016*, pages 445–454, 2016.
- [15] Mihai Cucuringu, Puck Rombach, Sang Hoon Lee, and Mason A Porter. Detection of core–periphery structure in networks using spectral methods and geodesic paths. *Eur. J. Appl. Math.*, 27(6):846–887, 2016.

- [16] Martin G. Everett and Stephen P. Borgatti. Peripheries of cohesive subsets. *Soc. Netw.*, 21(4):397 – 407, 2000.
- [17] Robert C Feenstra, Robert E Lipsey, Haiyan Deng, Alyson C Ma, and Hengyong Mo. World trade flows: 1962-2000. Working Paper 11040, National Bureau of Economic Research, January 2005.
- [18] S. Fortunato. Community detection in graphs. *Phys. Rep.*, 486:75–174, 2010.
- [19] Aric A. Hagberg, Daniel A. Schult, and Pieter J. Swart. Exploring network structure, dynamics, and function using NetworkX. In *Proc. of the 7th Python in Science Conference (SciPy2008)*, pages 11–15, CA USA, August 2008.
- [20] Petter Holme. Core-periphery organization of complex networks. *Phys. Rev. E*, 72:046111, Oct 2005.
- [21] L. Hubert and P. Arabie. Comparing partitions. *J Classif*, 2:193–218, 1985.
- [22] Brian Karrer and Mark EJ Newman. Stochastic blockmodels and community structure in networks. *Phys. Rev. E*, 83(1):016107, 2011.
- [23] Jon M Kleinberg. Authoritative sources in a hyperlinked environment. *Journal of the ACM (JACM)*, 46(5):604–632, 1999.
- [24] Jon M. Kleinberg. Authoritative sources in a hyperlinked environment. *J. ACM*, 46(5):604–632, September 1999.
- [25] Sadamori Kojaku. Cpalgorithm - python package. Github - <https://github.com/skojaku/core-periphery-detection>, Dec 2018.
- [26] Sadamori Kojaku and Naoki Masuda. Finding multiple core-periphery pairs in networks. *Phys. Rev. E*, 96:052313, Nov 2017.
- [27] Tarald O Kvalseth. Entropy and correlation: Some comments. *IEEE Transactions on Systems, Man, and Cybernetics*, 17(3):517–519, 1987.
- [28] James R Lee, Shayan Oveis Gharan, and Luca Trevisan. Multiway spectral partitioning and higher-order cheeger inequalities. *J. ACM*, 61(6):37, 2014.
- [29] S. H. Lee, M. Cucuringu, and M. A. Porter. Density-based and transport-based core-periphery structures in networks. *Phys. Rev. E*, 89, 2014.
- [30] Neng-Pin Lu. Using eigenvectors of perturbed and collapsed adjacency matrices to explore bowtie structures in directed networks. *J Chin Inst Eng*, 39(8):936–945, 2016.
- [31] Hong-Wu Ma and An-Ping Zeng. The connectivity structure, giant strong component and centrality of metabolic networks. *Bioinformatics*, 19(11):1423–1430, 2003.
- [32] J. B. MacQueen. Some methods for classification and analysis of multivariate observations. In L. M. Le Cam and J. Neyman, editors, *Proceedings of the fifth Berkeley Symposium on Mathematical Statistics and Probability*, volume 1, pages 281–297. University of California Press, 1967.



- [33] Marina Meilă. Comparing clusterings—an information based distance. *J. Multivar. Anal.*, 98(5):873 – 895, 2007.
- [34] M. Meilă and J. Shi. A random walks view of spectral segmentation. In *International Workshop on Artificial Intelligence and Statistics (AISTATS)*, 2001.
- [35] R. J. Mondragón. Network partition via a bound of the spectral radius. *J. Complex Netw.*, 5(4):513–526, 12 2016.
- [36] M. Newman. *Networks*. Oxford University Press, 2nd edition, 2018.
- [37] Pedregosa, F. et al. Scikit-learn: Machine learning in Python. *J. Mach. Learn. Res.*, 12:2825–2830, 2011.
- [38] Tiago P Peixoto. Efficient monte carlo and greedy heuristic for the inference of stochastic block models. *Phys. Rev. E*, 89(1):012804, 2014.
- [39] Tiago P. Peixoto. The graph-tool python library. *Figshare*, 2014.
- [40] Tiago P. Peixoto. Hierarchical block structures and high-resolution model selection in large networks. *Phys. Rev. X*, 4:011047, Mar 2014.
- [41] M. A. Porter, J.-P. Onnela, and P. J. Mucha. Communities in networks. *Notices Amer. Math. Soc*, 56:1082, 2009.
- [42] Karl Rohe, Tai Qin, and Bin Yu. Co-clustering directed graphs to discover asymmetries and directional communities. *Proc. Natl. Acad. Sci. U.S.A.*, 113(45):12679–12684, 2016.
- [43] Puck Rombach, Mason A Porter, James H Fowler, and Peter J Mucha. Core-periphery structure in networks (revisited). *SIAM Review*, 59(3):619–646, 2017.
- [44] Venu Satuluri and Srinivasan Parthasarathy. Symmetrizations for clustering directed graphs. In *Proc. of the 14th International Conference on Extending Database Technology*, pages 343–354. ACM, 2011.
- [45] Tom A.B. Snijders and Krzysztof Nowicki. Estimation and prediction for stochastic block-models for graphs with latent block structure. *J Classif*, 14(1):75–100, Jan 1997.
- [46] Wenli Tang, Liutao Zhao, Wei Liu, Yiping Liu, and Bo Yan. Recent advance on detecting core-periphery structure: a survey. *CCF Transactions on Pervasive Computing and Interaction*, pages 1–15, 2019.
- [47] F. Tudisco and D. J. Higham. A nonlinear spectral method for core–periphery detection in networks. *SIMODS*, 1:269–292, 2019.
- [48] J. van Lidth de Jeude, G. Caldarelli, and T. Squartini. Detecting core-periphery structures by surprise. *EPL (Europhysics Letters)*, 125(6):68001, apr 2019.
- [49] Jeroen van Lidth de Jeude, Riccardo Di Clemente, Guido Caldarelli, Fabio Saracco, and Tiziano Squartini. Reconstructing mesoscale network structures. *Complexity*, 2019.

- [50] Jaewon Yang and Jure Leskovec. Structure and overlaps of communities in networks. *arXiv preprint arXiv:1205.6228*, 2012.
- [51] R. Yang, L. Zhuhadar, and O. Nasraoui. Bow-tie decomposition in directed graphs. In *14th International Conference on Information Fusion*, pages 1–5, July 2011.
- [52] Xiao Zhang, Travis Martin, and Mark EJ Newman. Identification of core-periphery structure in networks. *Phys. Rev. E*, 91(3):032803, 2015.

# Supplementary Information

## A Alternative Definitions of Directed Core-Periphery

In the main text, we proposed a novel directed core–periphery structure, introduced methods to detect it, compared the performance of these methods on synthetic benchmarks, and explored this structure in real-world networks. While we find the extension of core–periphery to the directed case a natural one to consider and insightful in real-world data, there are other possible choices. To better understand the space of possible directed configurations that still maintain a core–periphery-like structure, we propose a set of criteria, and then enumerate all possible structures which satisfies these criteria.

We start with a partition of the vertex set into four potentially empty sets, which we call Core 1, Core 2, Periphery 1, and Periphery 2 (we suppress the corresponding number when there is only one set of its kind). For a directed core–periphery structure, we impose the following restrictions

1. There cannot be connections within or between periphery sets.
2. A periphery set must connect to exactly one core set.
3. Any pair of sets designated as core must connect to each other, must be connected internally, and each core set must be connected to at least one periphery set.
4. The structure can have no reciprocal edges between any two distinct blocks.

We detail below the structures that satisfy the above assumptions.

**(i) 1 Core set and 1 periphery set** We first consider the case of one core and one periphery set. As the core must connect internally, and the periphery set must connect to the core, there are two possible design matrices

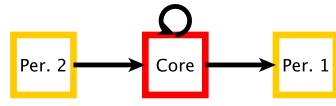
$$\begin{array}{cc|cc} & \text{Core} & \text{Periphery} & \\ \text{Core} & 1 & 1 & \\ \text{Periphery} & 0 & 0 & \end{array} \quad \begin{array}{c} \text{Core} \rightarrow \text{Per.} \end{array} \quad (\text{A.16})$$

$$\begin{array}{cc|cc} & \text{Core} & \text{Periphery} & \\ \text{Core} & 1 & 0 & \\ \text{Periphery} & 1 & 0 & \end{array} \quad \begin{array}{c} \text{Per.} \rightarrow \text{Core} \end{array} \quad (\text{A.17})$$

Directed core–periphery structure (A.16) and (A.17) represent an asymmetric flow between the core and the periphery, as a periphery either only sends or only receives links. This can be a flow of information, such as follower-only accounts in Twitter networks, or a flow of money such as peripheral banks in inter-bank networks who sell their loans to central banks.

**(ii) 2 Core sets and 1 periphery set** As we restrict the periphery set to connect to only one core, and each core set to connect to at least one periphery, there is no possible design matrices that satisfy these constraints.

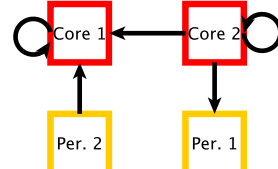
**(iii) 1 Core set and 2 periphery sets** In order for this case to make the structure identifiable, we exclude structures that can be obtained by splitting the peripheries of our 1 core and 1 periphery structures. Under this restriction, only one configuration is possible, namely having the peripheries connect in different directions. Below is the resultant design matrix for this structure.

	Core	Per. 1	Per. 2	
Core	1	0	1	
Per. 1	1	0	0	
Per. 2	0	0	0	

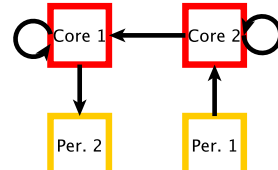
(A.18)

Directed core–periphery structure (A.18) is a particular instance of the well-known bow-tie structure, essentially having a set of vertices that only send material (content, money, etc.), and a set of vertices that only receive material; there are several known real world examples, namely of the internet in [10] and in biological networks [31].

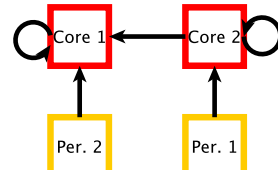
**(iv) 2 Core sets and 2 periphery sets** In the case of 2 core and 2 periphery sets, the cores must interconnect, and the link cannot be reciprocated, so that there is only one possible structure between the two core sets. By assumption, the periphery vertices only connect to one core set, and each core set must be connected to a periphery. Therefore, there are four possible such structures

	Core 1	Core 2	Per. 1	Per. 2	
Core 1	1	0	0	1	
Core 2	1	0	0	0	
Per. 1	0	1	0	0	
Per. 2	0	0	0	0	

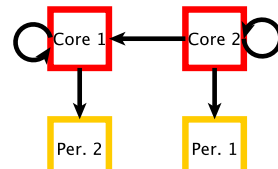
(A.19)

	Core 1	Core 2	Per. 1	Per. 2	
Core 1	1	0	0	0	
Core 2	1	1	1	0	
Per. 1	0	0	0	0	
Per. 2	1	0	0	0	

(A.20)

	Core 1	Core 2	Per. 1	Per. 2	
Core 1	1	0	0	0	
Core 2	1	1	0	0	
Per. 1	0	1	0	0	
Per. 2	1	0	0	0	

(A.21)

	Core 1	Core 2	Per. 1	Per. 2	
Core 1	1	0	0	1	
Core 2	1	1	1	0	
Per. 1	0	0	0	0	
Per. 2	0	0	0	0	

(A.22)

To the best of our knowledge, these structures have not been directly studied before. The directed core–periphery structure (A.20) is essentially a bow-tie in which the core can be split into

two sets, one which takes the incoming connections of the periphery vertices, and the remaining core set which sends links to the additional periphery set. This could be seen as a two-step process version of the bow-tie structure, in which material is taken in, processed, and then distributed to a second set that performs a similar action. In contrast, the structure (A.19), which is the one on which the main paper focuses, is not a simple extension of the bow-tie structure due to the fact that, contrary to bow-tie, the flow in (A.19) is not uni-directional.

## B Stochastic Block Model Fitting

In this section, we detail the algorithms for fitting a stochastic block model to the proposed structure.

### (a) HILLCLIMB Method

The first approach is HILLCLIMB from [45]. Our implementation is as follows.

1. Repeat the following procedure 10 times
  - (a) Assign all vertices to a random set from  $\mathcal{P}_{in}$ ,  $\mathcal{P}_{out}$ ,  $\mathcal{C}_{in}$  and  $\mathcal{C}_{out}$ .
  - (b) For a fixed number of repeats (5000 for results in the paper):
    - i. Compute the optimal value of  $p_1$  and  $p_2$  by looking at the density in both regions of the block structure, enforcing  $p_1 > p_2$ .
    - ii. Consider each vertex in a random order and place it in the set with the highest probability (using the fixed values of  $p_1$  and  $p_2$ ).
    - iii. If there are no changes to the vertex sets then exit the loop.
2. Select the partition with the largest likelihood.

To enforce the constraint that  $p_1 > p_2$ , we define  $p_1 = \max(p_1, p_2)$ , and  $p_2 = \min(p_1, p_2)$ . The algorithm differs slightly from [45], firstly as we have a fixed number of repeats, and secondly as we fit a likelihood with fixed set sizes and only two parameters to estimate,  $p_1$  and  $p_2$ .

### (b) MAXLIKE Method

We implemented MAXLIKE from [22] as follows.

1. Assign all vertices to a random set (CURRENTPARTITION).
2. Calculate the likelihood of the random partition, and store it and the partition itself in BESTPARTITION.
3. Make a list LIST1 of all vertices.
4. Find the vertex in LIST1 for which the movement to a new set will increase the likelihood the most (or decrease the least). Perform the move and remove the vertex from LIST1.
5. If the likelihood of the current partition is larger than BESTPARTITION then replace BESTPARTITION with the current partition.
6. If LIST1 is not empty go to **iv**.

7. If BESTPARTITION has improved since **3** then set CURRENTPARTITION to BESTPARTITION and go to **3**.
8. Return BESTPARTITION.

### (c) Computational Complexity

There is a considerable difference in computational cost between the two likelihood approaches. In a naïve implementation, one pass of HILLCLIMB takes on the order of  $O(m)$  to compute the parameters  $p_1$  and  $p_2$  (each edge must be considered), and  $O(k_i)$  to update each vertex (querying membership of each neighbour) which overall is again  $O(m)$ . As there is a fixed number of iterations, this leads to  $O(m)$  overall. MAXLIKE has a larger computational cost, with the naïve approach to assessing whether to change a vertex’s set having a complexity of  $O(k_i)$  (as before). Further, as we consider moving each unmoved vertex each time we run step 4, and step 4 is ran  $n$  times, each iteration considers moving a vertex  $\binom{n+1}{2}$  times. If we store the neighbourhood structure of each vertex and update it whenever there are changes, we can reduce the complexity of exploring changing a vertices community to  $O(1)$  with the addition of  $O(k)$  when changing the structure, leading to an overall complexity of  $O(n^2 + m)$ .

## C Selection and Performance of Different Variants of the LOWRANK and the HITS Methods

Several methodological choices were made during the development stage of HITS, LOWRANK, and ADVHITS methods, based on their relative performance on our synthetic benchmarks, as follows. The LOWRANK method can be broken down into the following steps.

1. Construct a rank-2 approximation of the observed graph adjacency matrix.
2. Construct vertex scores from the low-rank approximation.
3. Cluster the vertices by applying k-means++ to the scores.

For the low-rank approximation step, following [15], we considered adding a threshold to convert the low-rank approximation from a fully connected weighted directed (albeit low-rank) graph to a directed unweighted sparse graph, which may be computationally advantageous for large graphs. For the purpose of choosing whether to apply a threshold or not in the analysis shown in the main text, we compared the non-thresholded case to a threshold of 0.5.

For the scoring step described in the main text, we use the scores  $\mathbf{C}_{in}^{LR}$ ,  $\mathbf{C}_{out}^{LR}$ ,  $\mathbf{P}_{In}^{LR}$  and  $\mathbf{P}_{Out}^{LR}$ . This formulation is degree-based and does not leverage other network information such as the score of the neighbours of a vertex. In this section, we consider two scoring variants for the periphery sets, the first leveraging network information and the second further exploiting the low-rank structure. For the first alternative formulation, heuristically, a vertex  $i$  should have a high  $\mathcal{P}_{in}$  score if

1. it has in-coming edges from vertices that have high  $\mathcal{C}_{out}$  scores;
2. it does not have high  $\mathcal{C}_{out}$ ,  $\mathcal{C}_{in}$  and  $\mathcal{P}_{out}$  scores.

Additionally, a vertex  $i$  should have a high  $\mathcal{P}_{out}$  score if

1. it has out-going edges to vertices that have high  $\mathcal{C}_{in}$  scores;
2. it does not have high  $\mathcal{C}_{out}$ ,  $\mathcal{C}_{in}$  and  $\mathcal{P}_{in}$  scores.

Combing these, we propose the following alternative scoring scheme

$$P_{In}^{LR-Alt}(i) = \sum_{j=1, j \neq i}^n \left( -\widehat{A}_{ij} C_{In}^{LR}(j) - \widehat{A}_{ij} C_{Out}^{LR}(j) + \widehat{A}_{ji} C_{In}^{LR}(j) - \widehat{A}_{ji} C_{Out}^{LR}(j) \right), \quad (C.23)$$

$$P_{Out}^{LR-Alt}(i) = \sum_{j=1, j \neq i}^n \left( \widehat{A}_{ij} C_{In}^{LR}(j) - \widehat{A}_{ij} C_{Out}^{LR}(j) - \widehat{A}_{ji} C_{In}^{LR}(j) - \widehat{A}_{ji} C_{Out}^{LR}(j) \right). \quad (C.24)$$

For the second score variant, we further leverage the low-rank structure. Rather than assigning the scores based on degrees, we assign scores from the left and right singular vectors in the rank-2 decomposition, either using the values directly or by first re-scaling by the square root of the singular values.

To decide which approach to use in the main paper, we assessed the variants without thresholds and with a threshold of 0.5 for the original and alternative scoring scheme (thresholding does not impact the direct singular value schemes). We selected the approach suggested in the main paper as it has the best overall performance (although there are narrow regions with very differently-sized sets and a high network density where other approaches may perform better). Similarly to the low-rank structure, we also considered two variants of the HITS method, based on the alternative scoring in Eqs. (C.23) and (C.24). The scoring scheme we presented in the main body outperforms the alternatives on all three benchmarks.

## D Synthetic Benchmarks

In this section, we present additional content and results which relate to our synthetic benchmarks. We first detail the ARI similarity measure used in the main document, as well as alternative similarity measures one could use (Section D(a)). Next, we present results for alternative network sizes (Section D(b)), timing results for Benchmark 1 (Section D(c)), and finally, results using alternative similarity measures (Section D(d)).

### (a) Similarity Measures

**Adjusted Rand index** The Adjusted Rand Index (ARI) [21] measures the similarity between two partitions of a data set. Let  $V = (v_1, v_2, \dots, v_n)$  be a set of vertices we wish to cluster, let  $X = (X_1, X_2, X_3, X_4)$  be a partition of  $V$  into four clusters, and let  $Y = (Y_1, Y_2, Y_3, Y_4)$  be the ideal partition. We let  $a$  be the number of vertex pairs that are placed in the same set of  $X$  and in the same set of  $Y$ ;  $b$  be the number of vertex pairs that are placed in the same set of  $X$  but in different sets of  $Y$ ;  $c$  be the number of vertex pairs that are placed in different sets of  $X$  but in the same set of  $Y$ ;  $d$  be the number of vertex pairs that are placed in different sets of  $X$  and in different sets of  $Y$ . The Adjusted Rand Index [21] is

$$\text{ARI} = \frac{\binom{n}{2}(a+d) - [(a+b)(a+c) + (c+d)(b+d)]}{\binom{n}{2}^2 - [(a+b)(a+c) + (c+d)(b+d)]}.$$

The Adjusted Rand Index (ARI) is bounded by  $\pm 1$  with an expected value of 0. An ARI close to 1 indicates an almost perfect match between the two partitions, whereas an ARI close to -1 indicates that the agreements between two partitions is less than what is expected from random labellings, which has an ARI of 0.

**Normalised Mutual Information (NMI) and Variation of Information (VOI)** Both of these measures are based on the concept of entropy and mutual information [12]. For a random variable  $X$  which takes values in a discrete set  $\mathcal{S}_X$ , and a random variable  $Y$  which take values in a discrete set  $\mathcal{S}_Y$  [12], the entropy of  $X$  is

$$H(X) = - \sum_{a \in \mathcal{S}_X} P(X = a) \log(P(X = a))$$

and the mutual information  $MI(X, Y)$  of  $X$  and  $Y$  is

$$MI(X, Y) = \sum_{a \in \mathcal{S}_X} \sum_{b \in \mathcal{S}_Y} P(X = a, Y = b) \log \left( \frac{P(X = a, Y = b)}{P(X = a)P(Y = b)} \right).$$

The variation of information  $VOI(X, Y)$  is defined as

$$VOI(X, Y) = H(X) + H(Y) - 2MI(X, Y),$$

see for example [33]. Thus, if  $MI(X, Y) = H(X) = H(Y)$ , indicating that the information in  $X$  is perfectly captured by the information in  $Y$ ,  $VOI(X, Y)$  would have a value of 0. If  $MI(X, Y) = 0$ , then  $VOI(X, Y)$  takes the largest possible value. Normalised mutual information  $NMI(X, Y)$  is defined in [27] as

$$NMI(X, Y) = \frac{2MI(X, Y)}{H(X) + H(Y)}$$

Again, if  $H(X) = H(Y) = MI(X, Y)$ , then  $NMI(X, Y) = 1$ , whereas if  $MI(X, Y) = 0$ , then  $NMI(X, Y) = 0$ .

## (b) Additional ARI Results

Here we show the performance on Benchmark 1 and Benchmark 2 of our approaches for  $n = 400$  in comparison to  $n = 1000$  (to show the effect of different networks sizes), and additional Benchmark 2 contour plots displayed at ARI=0.9 in contrast to the ARI=0.75 (to show the effect of different contour thresholds for a given network size).

The comparison for graphs of different size is shown in Fig. SI 1 (Benchmark 1); Fig. SI 2 (Benchmark 2) and Fig. SI 3 (Benchmark 3). In Benchmark 1 and 2 the results are qualitatively similar between the graph sizes with methods failing in the same order and in the same manner, although the range of values where this failure occurs shifts. This is expected as there is additional information present in larger graphs, so we would expect smaller values of  $p$  to have potentially larger effects on performance (up to detectability limits). We observe a similar effect in Benchmark 3 for  $n = 1000$ , with the increased network size (and fixed value of  $p = 0.1$ ) many methods perform better over the range of block sizes, although we note that we do observe a similar decay in the performance of ADVHITS. The 0.75 and 0.9 contours for ARI are shown in (Fig. SI 2). The results are broadly consistent, with similar performance for many regimes in the 0.9 contour but a much larger performance difference in the 0.75 contour.



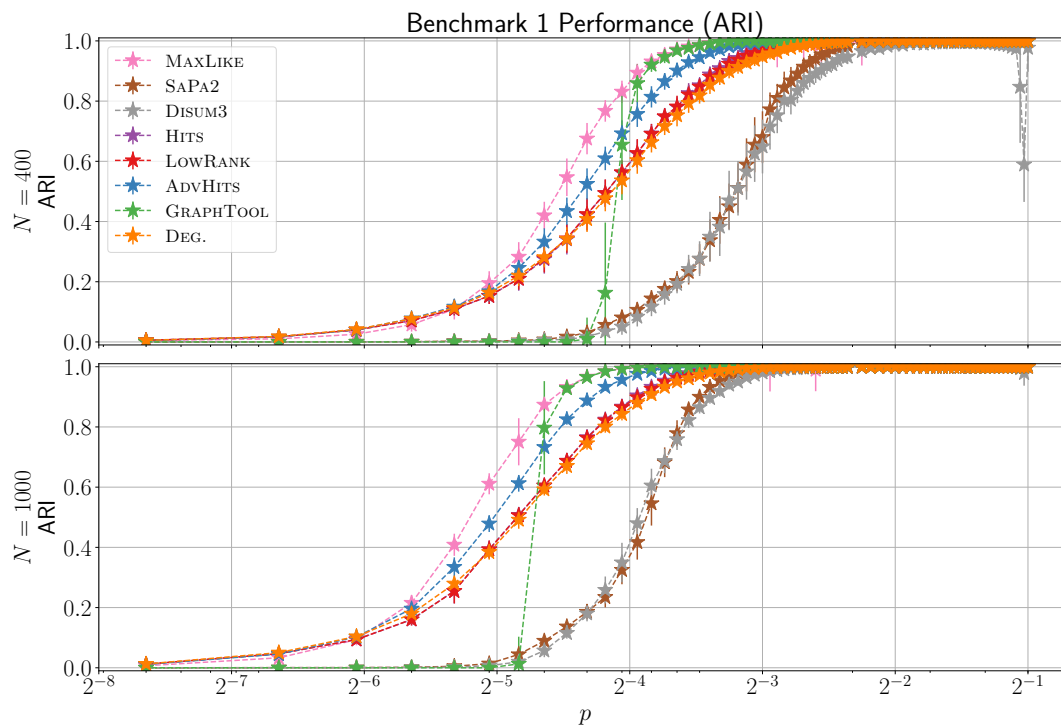


Figure SI 1: Performance on Benchmark 1. The ARI between the planted partition of the graph and the partition detected by each method, with the upper, respectively lower, panel showing results for networks of size  $n = 1000$ . On the  $x$  axis, we vary the parameter  $p$  on a log scale. Error bars are one sample standard deviation.

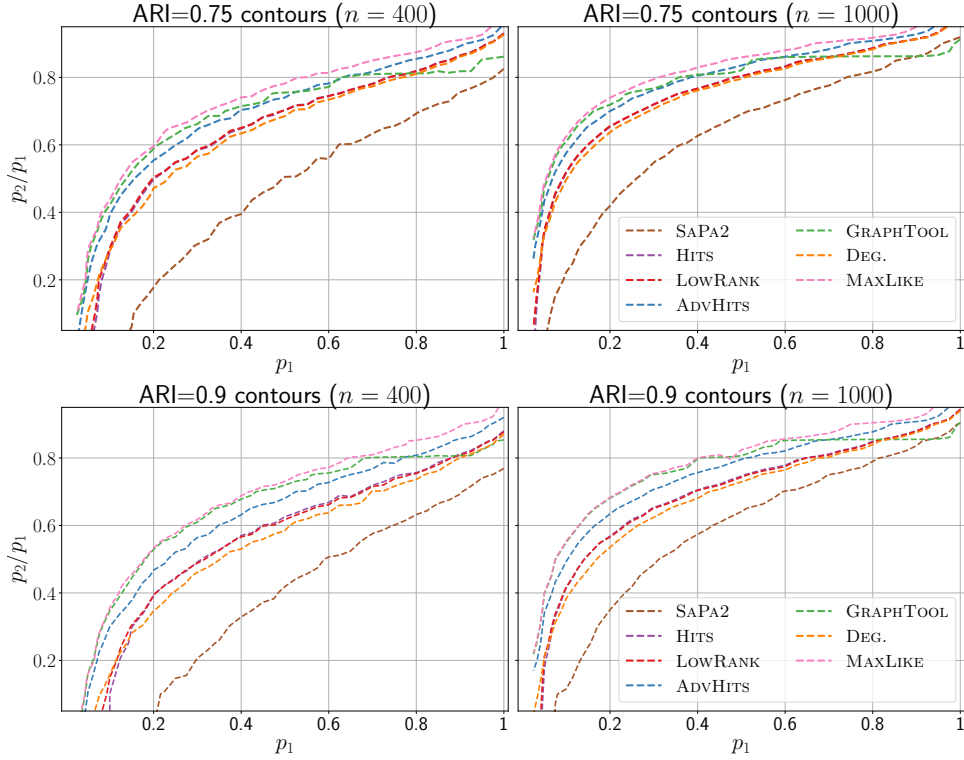


Figure SI 2: Contour plot of ARI=0.75 and ARI=0.9 on Benchmark 2. For this plot, we calculate the average ARI over 10 networks of size 400 (left panel) and 1000 (right panel) varying  $p_1 \in \{0.025, 0.05, \dots, 1.0\}$  and  $\frac{p_2}{p_1} \in \{0, 0.05, 0.1, \dots, 0.95\}$ , and then display the contours corresponding to an average ARI of 0.75. We note that the fast methods HITS and LOWRANK outperform the comparisons DEG. and SAPA2, although they are hard to distinguish due to similar performance. AdvHITS also outperforms the fast comparisons. MAXLIKE has similar performance to GRAPHTOOL, but like AdvHITS outperforms for larger values of  $p_1$ .

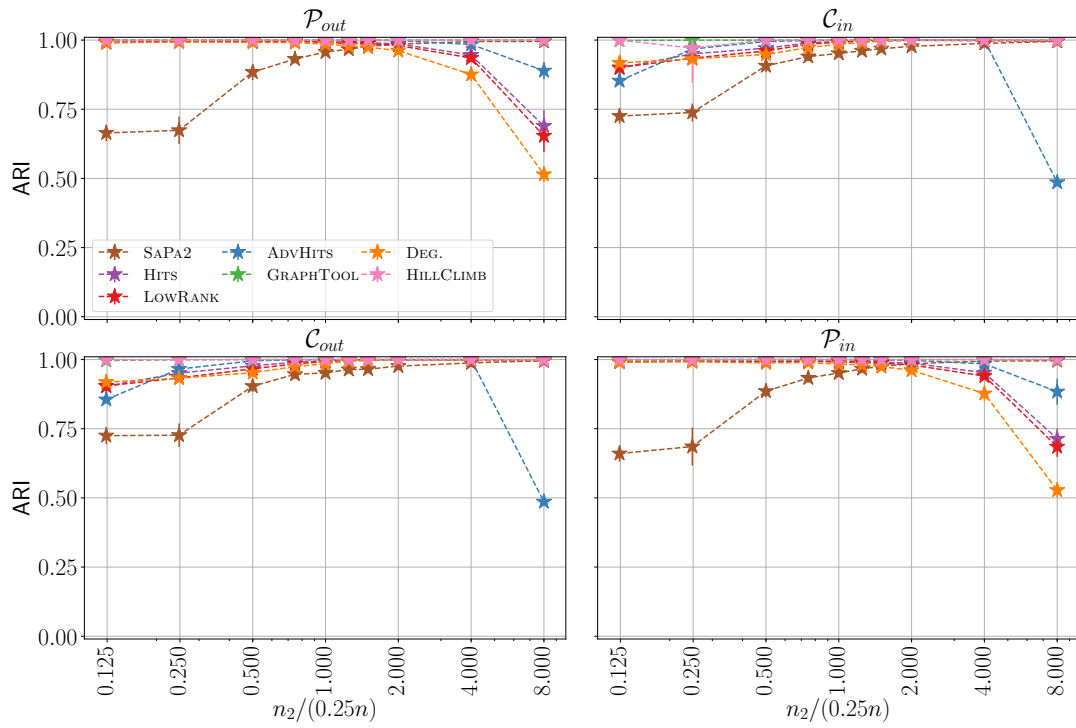


Figure SI 3: Performance of all methods on Benchmark 3 with sets of different sizes using ARI, for  $n = 1000$ . We fix  $p = 0.1$  and the size of 3 sets at  $n/4$ , and then measure the ability of each method to detect the sets when the size of the final set is varied.

### (c) Run Time On Synthetic Networks

The two panels of Fig. SI 4 show the run time of each of the methods. We note that the time comparison is advisory as this calculation was performed on a Azure Virtual Machine. To mitigate the effects of hyperthreads we used half of the available vCPUs but we cannot control for other users present on the same physical hardware. Further, different approaches are implemented in different languages, with the matrix based methods (HITS, ADVHITS, SAPA, DiSUM, HITS, and LOWRANK) being implemented in Python using NumPy and SciPy vectorised matrix operations, GRAPHTOOL in C++ with Python wrapping<sup>1</sup>, and the likelihood methods are implemented in pure Python ran under cPython with the exception of MAXLIKE for  $n = 1000$  which was ran under PyPy [6]. We note that when testing these methods under PyPy we obtain a  $\approx 10x$  speed up on the cPython times. Finally, we note that the implementation of SAPA, DiSUM, HITS, LOWRANK are relatively naïve, and could be improved, for example, by exploiting the specialised matrix construction code we use in ADVHITS.

We observe that the performance of many of the methods is relatively constant with respect to  $p$ , with an increase in run time when  $p$  is small. This behaviour is especially pronounced in ADVHITS with comparatively fast times for the easier graphs, and slower times for the harder graphs, which is likely to be because the method falls back to the single vertex update scheme for small values of  $p$ . This is also likely to be related to the error bars (one sample standard deviation), which increase for low  $p$  in ADVHITS for  $n = 400$ . We note that ADVHITS would have similar time complexity to the PyPy version of HILLCLIMB (with 10 repeats) but have substantially better time complexity than MAXLIKE, highlighting that the ADVHITS approach is a medium speed approach in contrast to the fast approaches.

### (d) Benchmark Results for VOI and NMI

**Benchmark 1** The NMI and VOI results for Benchmark 1 can be found in Fig. SI 5. Broadly, the results are qualitative similar to the ARI results. For both NMI and VOI, SAPA2 and DiSUM, are outperformed by all other methods, which is consistent with the results of ARI. Similarly ADVHITS and MAXLIKE outperform clustering based on degree in all cases, with the HITS and LOWRANK methods performing at least as well as clustering based on degree. We also observe an equivalent result performance result for ADVHITS, with a performance improvement over LOWRANK and HITS methods, but outperformed by MAXLIKE. We only show the results for  $n = 1000$ ; the results for  $n = 400$  are similar.

We highlight the VOI results for GRAPHTOOL. It outperforms the other methods for  $p < 2^{-6}$  whereas ARI and NMI show precisely the opposite performance. This discrepancy may be related to the effect that placing almost all vertices into one set has on the similarity measures. Indeed, Table 2 shows the average size of the largest set in LOWRANK, ADVHITS and GRAPHTOOL. For LOWRANK and ADVHITS the average largest set size is close to a equal division into 4 equally-sized sets, whereas GRAPHTOOL incorrectly places most of the vertices in a single set for  $p < 0.04 \approx 2^{-4.64}$ . With most vertices in the GRAPHTOOL partition in one set, the entropy will be close to 0, as  $-\log(1 - \epsilon) \approx 0$ , thus, as mutual information is by definition less than the entropy, the VOI becomes close to the entropy of the almost constant sequence, which is equal to  $-\log_2(0.25) = 2$ , a relatively high value.

---

<sup>1</sup>The GRAPHTOOL timings also contains the C++ graph construction, and the matrix approaches timings contain the matrix construction

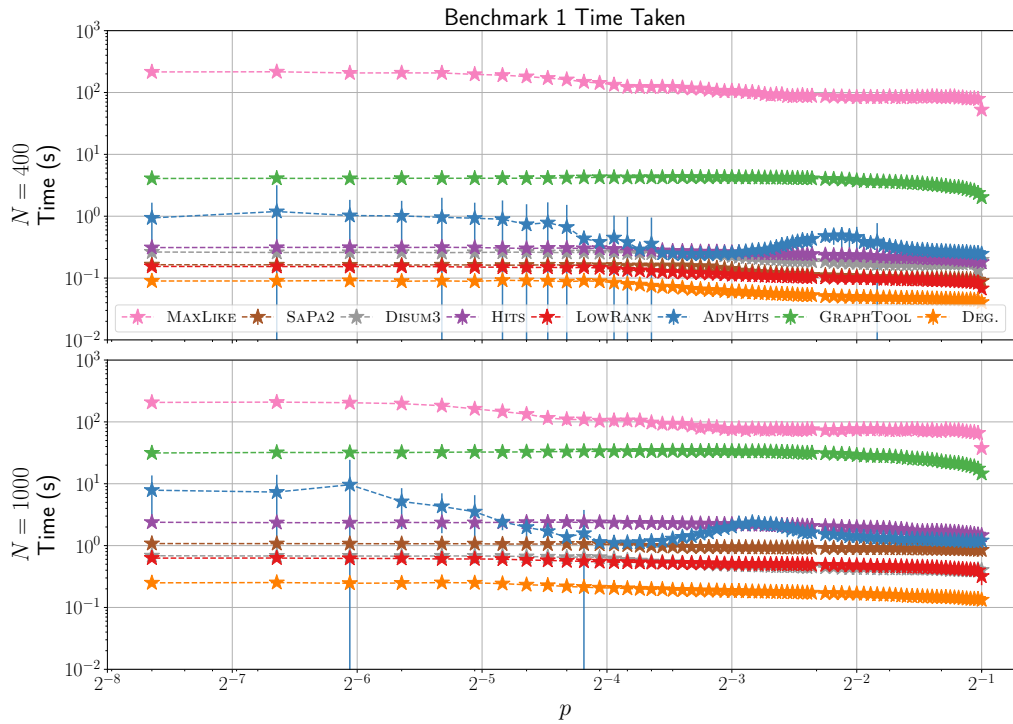


Figure SI 4: Time taken by all methods on Benchmark 1 with the upper, respectively lower, panel showing results for networks of size  $n = 400$ , respectively  $n = 1000$ . On the  $x$  axis, we vary the parameter  $p$ , with values close to 0 more difficult to detect than higher values of  $p$ . The timing for MAXLIKE for  $n = 1000$  was ran under PyPy, a faster Python interpreter, to highlight the possible speed up.

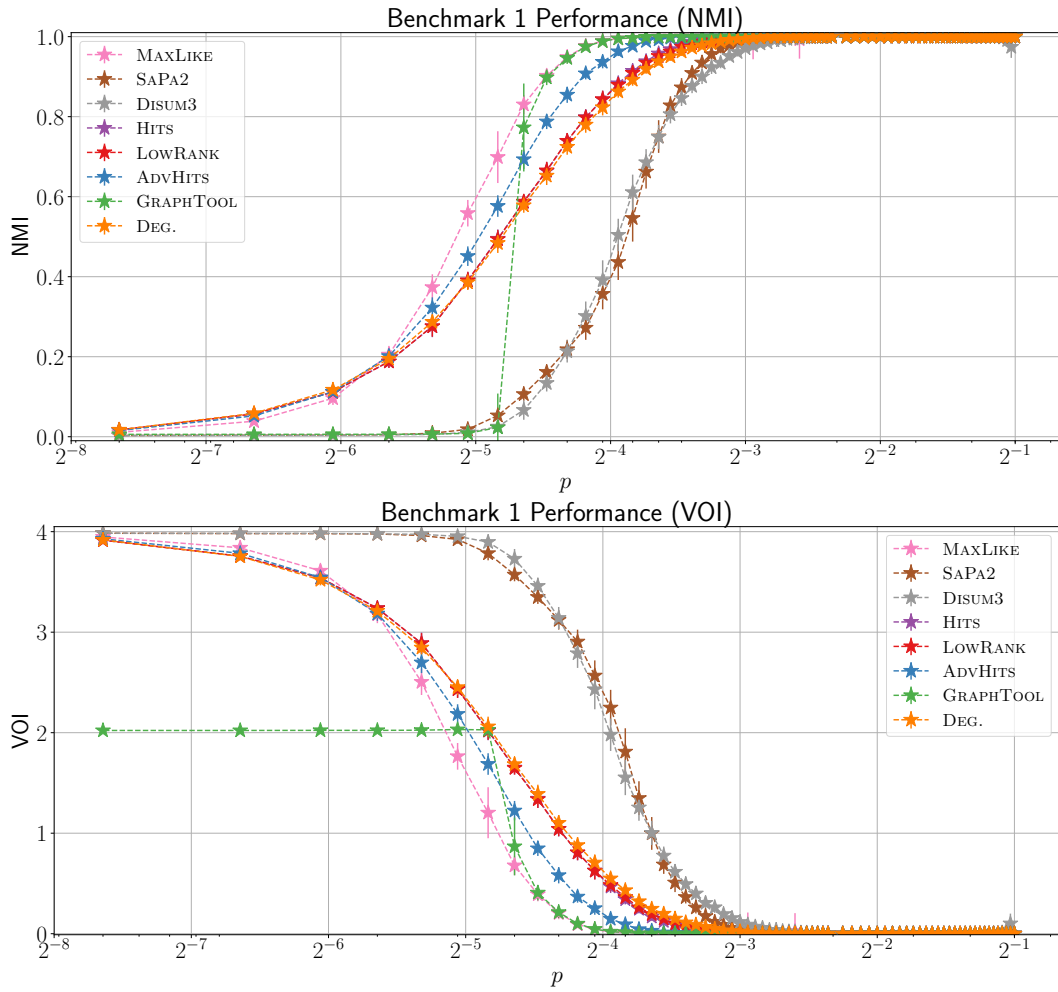


Figure SI 5: Performance on Benchmark 1. The NMI (**Top Panel**) and VOI (**Bottom Panel**) between the underlying partition of the graph and the detected partition for  $n = 1000$ . On the  $x$  axis, we vary the parameter  $p$ , with values close to 0 more difficult to detect than higher values of  $p$ . Error bars are one sample standard deviation.

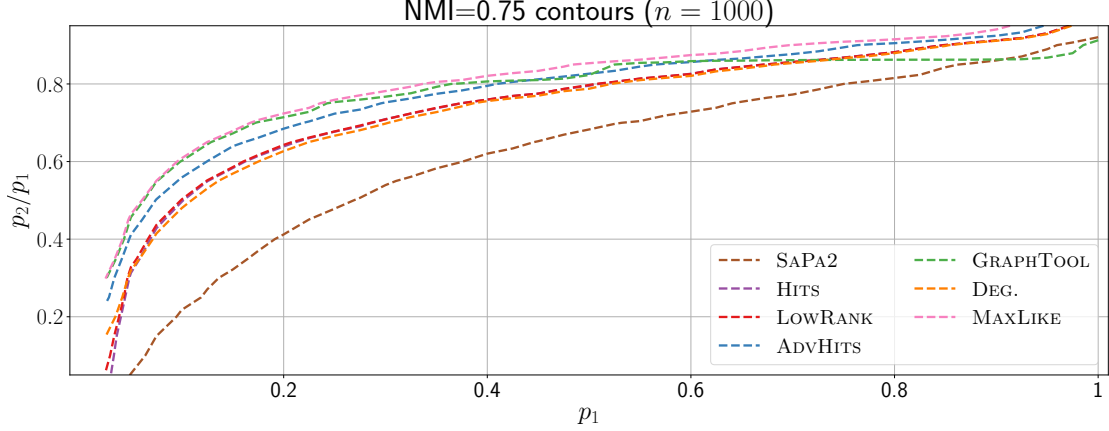


Figure SI 6: Contour plot of  $NMI=0.75$  on the Benchmark 2. For this plot, we calculate the average NMI over 10 networks of size 1000 varying  $p_1 \in \{0.025, 0.05, \dots, 1.0\}$  and  $\frac{p_2}{p_1} \in \{0, 0.05, 0.1, \dots, 0.95\}$ , and then display the contours corresponding to an average NMI of 0.75 and 0.9.

The behaviour of NMI on GRAPHTOOL can also be similarly explained, as mutual information is close to 0, NMI then also becomes close to 0.

**Benchmark 2** For brevity, in the main text we considered contour plots for a fixed value of ARI. In this section, we consider alternative similarity measures. We again only show the results for  $n = 1000$ ; the results for  $n = 400$  are similar.

The NMI contours, displayed in Fig. SI 6, tell a broadly similar story to the ARI results (Fig. SI 2) with the methods having the same ordering and performance as we observe ARI. The VOI contours, displayed in Fig. SI 7, show broadly consistent findings but with a few small deviations.

**Benchmark 3** The results for Benchmark 3 be seen in Fig. SI 8. They are broadly consistent across each of the similarity measures, although there is a small deviation with the performance of ADVHITS for  $\frac{n_2}{n} > 2$ . The information theoretic measures (NMI and VOI) yield a slightly higher performance for ADVHITS (in comparison to the controls) than the ARI. In both cases, the performance of ADVHITS collapses in this region.

### (e) Performance of DISUM and SAPA variants

As alluded to in the main text we consider a small number of variants of our spectral comparison methods and only display the best performing method. In this section we discuss the other variants we considered on each of our benchmarks.

**SAPA Variants** From [44], SAPA employ a similarity measure using two different types of symmetrisations for directed (asymmetric) adjacency matrices, namely bibiometric symmetrisation and degree discounted symmetrisation. We use them here to construct two variants of SAPA, SAPA1 and SAPA2, which we then cluster. They are defined as follows:

$n$	$p$	LOWRANK	ADVHITS	GRAPHTOOL
1000	0.050	260.8	264.42	252.62
1000	0.045	264.82	270.92	255.62
1000	0.040	270.74	279.6	298.68
1000	0.035	274.9	288.5	980.24
1000	0.030	280.62	295.52	995.42
1000	0.025	286.64	298.72	996.56
1000	0.020	290.64	292.18	996.88
1000	0.015	290.4	282.16	996.86
1000	0.010	296.2	282.18	997.0
1000	0.005	298.54	283.1	997.0

Table 2: Average (mean) size of the largest set in the detected partition in Benchmark 1. Note that the maximum achievable set size for a division into 4 non empty sets is  $1000 - 1 - 1 - 1 = 997$ .

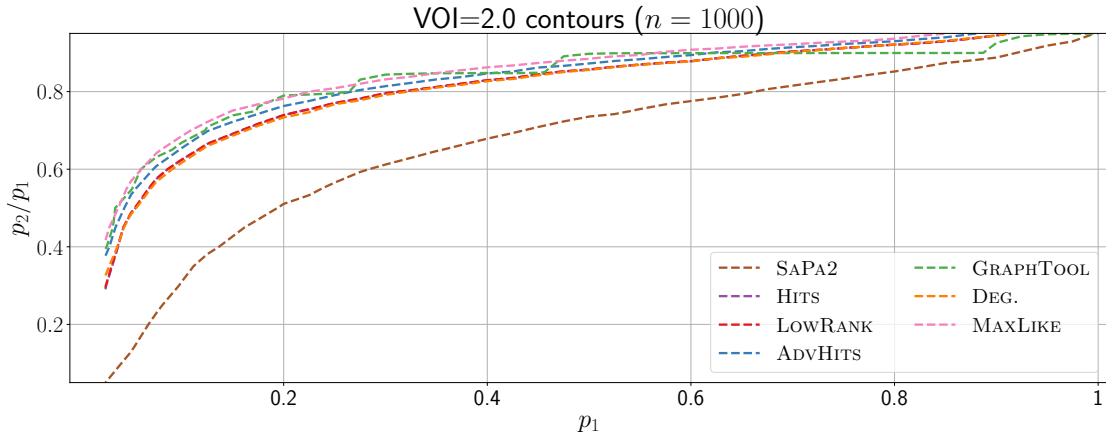


Figure SI 7: Contour plot of VOI=2.00 a on the Benchmark 2. For this plot, we calculate the average VOI over 10 networks of size 1000 varying  $p_1 \in \{0.025, 0.05, \dots, 1.0\}$  and  $\frac{p_2}{p_1} \in \{0, 0.05, 0.1, \dots, 0.95\}$ , and then display the contours corresponding to an average VOI of 2.0.



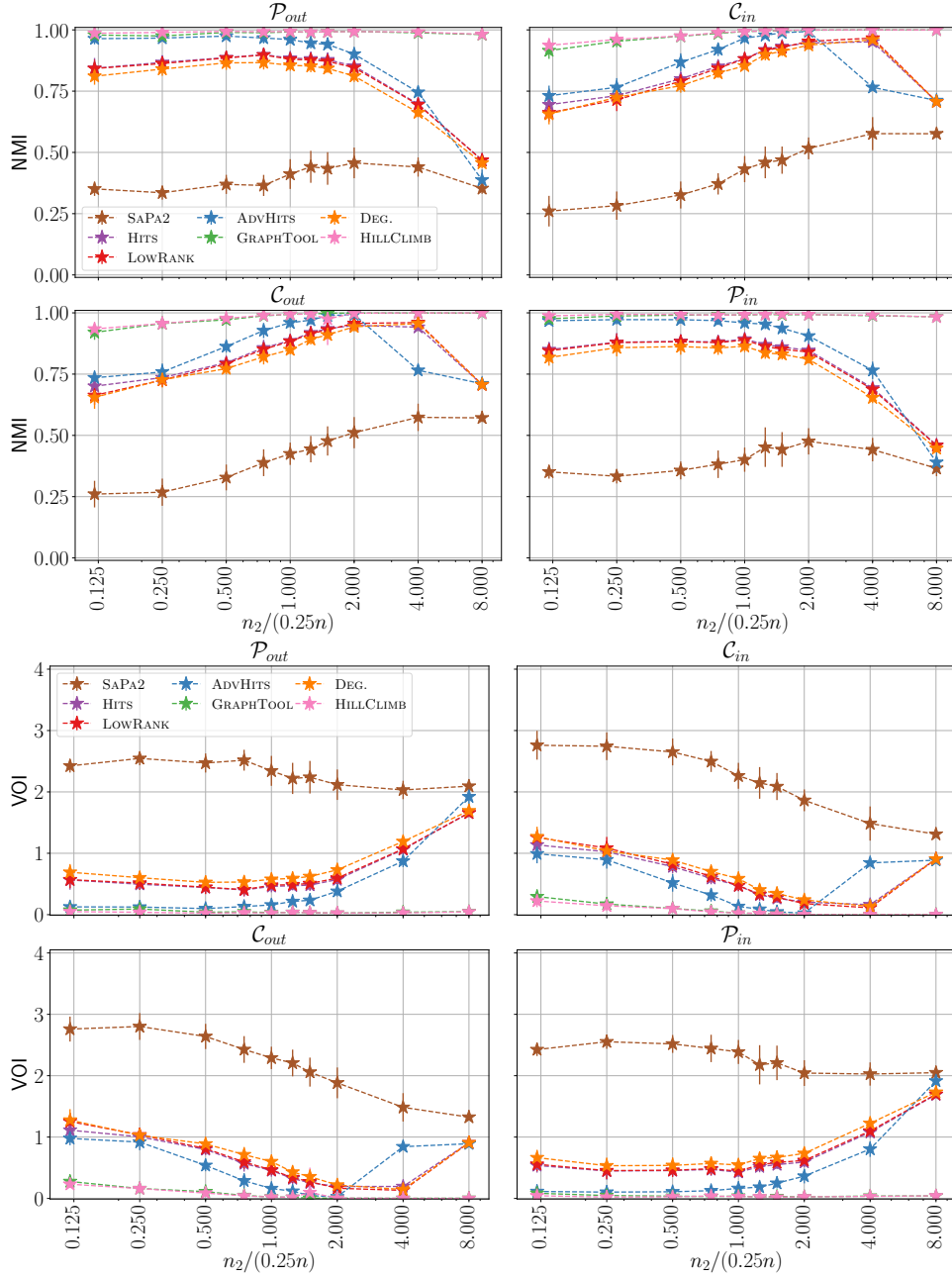


Figure SI 8: Performance of all methods on Benchmark 3 with sets of different sizes using NMI (**Top Panel**), and VOI (**Bottom Panel**). We fix  $p = 0.1$  and the size of 3 sets at  $n/4$ , and then measure the ability of each method to detect the sets when the size of the final set is varied.

1. SAPA1 - Bibiometric symmetrisation:  $A_I A_I^T + A_I^T A_I$
2. SAPA2 - Degree discounted:  $D_o^{-0.5} A D_i^{-0.5} A^T D_o^{-0.5} + D_i^{-0.5} A D_o^{-0.5} A^T D_i^{-0.5}$

where  $D_i$  is a diagonal matrix with the in-degrees on the diagonal,  $D_o$  is an diagonal matrix with the out-degrees on the diagonal,  $A_I = A + I$ , where  $I$  is the identity matrix. In the original formulation of SAPA, these similarity matrices were then clustered via various clustering algorithms. Instead, we use the same kmeans++ pipeline that we leverage for other results.

**DiSUM Variants** The second fast approach, DiSUM from [42], clusters the graph using the left and right singular vectors of the regularised and degree normalised adjacency matrix  $((k_i^{out} + \frac{m}{n})(k_i^{in} + \frac{m}{n}))^{-1/2} A_{ij}$ . The original approach in [42], performed a column and row clustering, as we are comparing to a full network clustering. We consider to 4 different variants of this approach:

1. DiSUM1 A row clustering into 4 sets,
2. DiSUM2 A column clustering into 4 sets,
3. DiSUM3 A combined row and column clustering into 4 sets (using the concatenation of the left and right singular vectors),
4. DiSUM4 Combining a row clustering into 2 sets with a column clustering into 2 sets to obtain 4 resultant sets (with each set defined by the intersection of a pair of sets from the different clusterings). Note, we use a separate row and column clustering rather than the combined clustering in [42].

We again cluster the resulting vectors using our standard pipeline i.e. k-means++.

**Results** Unlike in previous cases as this is a comparison method rather than computing an independent set of networks we display the method that performs best on our benchmark networks (results not shown).

We observe that SAPA2 and DiSUM3 outperform there counterparts on Benchmark 1; Benchmark 2 (where the other approaches are below the threshold). In Benchmark 3 DiSUM4 outperforms DiSUM3, for large differences in group sizes. However, given that the DiSUM3 performs reasonably and outperforms DiSUM4 considerably in the Benchmark 1 and Benchmark 2, we select this as our overall DiSUM method.

## E Political Blogs: Additional Results

In this section, we present additional results on the political blogs data set. We first explore the relationship between the sets we uncover and the political division of the network. Second we relate it to undirected core-periphery structure.

In the main paper we state that the partitions from ADVHITS and MAXLIKE are related to the political division into liberals (Left) and conservative (Right) blogs, but are not purely a function of it. Figure SI 9 gives the confusion matrices between each of our divisions and the political division. We observe that with the exception of HITS, the sets divide into two roughly similarly sized sets. These sets are not in 1-1 relationship with the Left/Right division of the blogs. Hence there is evidence that the sets also relate to structural properties of the vertices.

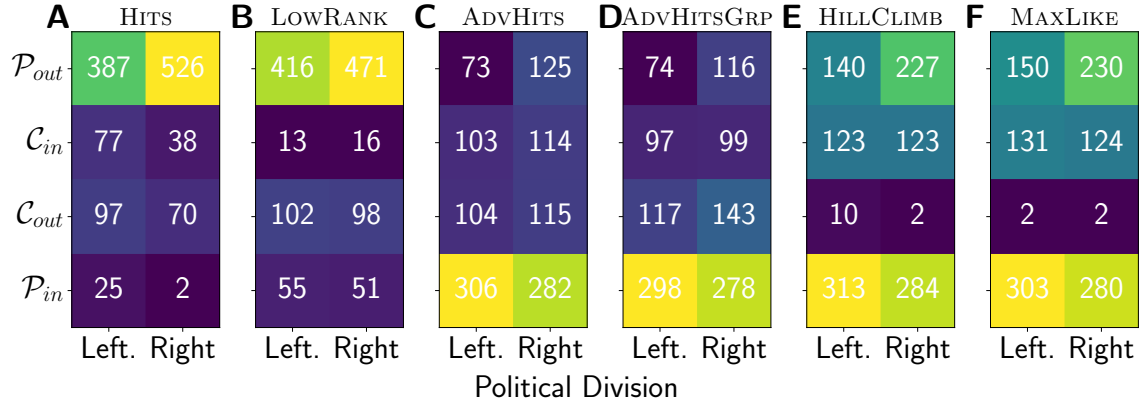


Figure SI 9: Each panel shows the confusion table of the detected sets by each method and the division into left and right leaning political blogs. Colour scales are different in each plots and are designed to show the differences within a panel.

Next we compare the division obtained using our approaches with the division found using the classical core–periphery approach. The results can be seen in Fig. SI 10. We note that the split of the undirected core into  $\mathcal{C}_{in}$  and  $\mathcal{C}_{out}$  and the split of the undirected periphery into  $\mathcal{P}_{in}$  and  $\mathcal{P}_{out}$  is present in ADVHITS and ADVHITSGRP.

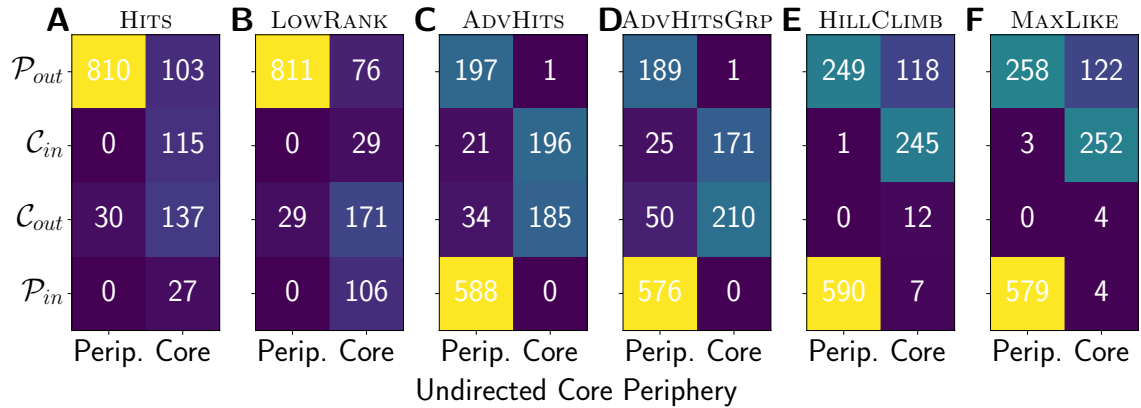


Figure SI 10: Each panel shows the confusion table of the detected sets by each method and the division into the undirected core–periphery structure. Colour scales are different in each plot, and are designed to show the differences within a panel.